

See discussions, stats, and author profiles for this publication at: <http://www.researchgate.net/publication/264864665>

# Laminar and Neurochemical Organization of the Dorsal Cochlear Nucleus of the Human, Monkey, Cat, and Rodents

ARTICLE *in* THE ANATOMICAL RECORD ADVANCES IN INTEGRATIVE ANATOMY AND EVOLUTIONARY BIOLOGY · OCTOBER 2014

Impact Factor: 1.54 · DOI: 10.1002/ar.23000

---

CITATION

1

READS

36

10 AUTHORS, INCLUDING:



[Nadav Weinstock](#)

University at Buffalo, The State University of ...

4 PUBLICATIONS 25 CITATIONS

[SEE PROFILE](#)



[Senthilvelan Manohar](#)

University at Buffalo, The State University of ...

30 PUBLICATIONS 308 CITATIONS

[SEE PROFILE](#)



[Sandra Witelson](#)

McMaster University

47 PUBLICATIONS 3,989 CITATIONS

[SEE PROFILE](#)

# Laminar and Neurochemical Organization of the Dorsal Cochlear Nucleus of the Human, Monkey, Cat, and Rodents

JOAN S. BAIZER,<sup>1\*</sup> KEIT MEN WONG,<sup>1</sup> NICHOLAS A. PAOLONE,<sup>1</sup>  
NADAV WEINSTOCK,<sup>1</sup> RICHARD J. SALVI,<sup>2</sup> SENTHILVELAN MANOHAR,<sup>2</sup>  
SANDRA F. WITELSON,<sup>3</sup> JAMES F. BAKER,<sup>4</sup> CHET C. SHERWOOD,<sup>5</sup>  
AND PATRICK R. HOF<sup>6</sup>

<sup>1</sup>Department of Physiology and Biophysics, University at Buffalo, Buffalo, New York

<sup>2</sup>Department of Communicative Disorders and Sciences, Center for Hearing and Deafness, University at Buffalo, Buffalo, New York

<sup>3</sup>Department of Psychiatry and Behavioural Neurosciences, Michael G. DeGroote School of Medicine, McMaster University, Hamilton, Ontario, Canada

<sup>4</sup>Department of Physiology, Northwestern University Medical School, Chicago, Illinois

<sup>5</sup>Department of Anthropology, The George Washington University, Washington, DC

<sup>6</sup>Fishberg Department of Neuroscience and Friedman Brain Institute, Icahn School of Medicine at Mount Sinai, New York, New York

---

---

## ABSTRACT

The dorsal cochlear nucleus (DCN) is a brainstem structure that receives input from the auditory nerve. Many studies in a diversity of species have shown that the DCN has a laminar organization and identifiable neuron types with predictable synaptic relations to each other. In contrast, studies on the human DCN have found a less distinct laminar organization and fewer cell types, although there has been disagreement among studies in how to characterize laminar organization and which of the cell types identified in other animals are also present in humans. We have reexamined DCN organization in the human using immunohistochemistry to analyze the expression of several proteins that have been useful in delineating the neurochemical organization of other brainstem structures in humans: nonphosphorylated neurofilament protein (NPNFP), nitric oxide synthase (nNOS), and three calcium-binding proteins. The results for humans suggest a laminar organization with only two layers, and the presence of large projection neurons that are enriched in NPNFP. We did not observe evidence in humans of the inhibitory interneurons that have been described in the cat and rodent DCN. To compare humans and other animals directly we used immunohistochemistry to examine the DCN in the macaque monkey, the cat, and three rodents. We found similarities between macaque monkey and human in the expression of NPNFP and nNOS, and unexpected differences among species in the patterns of expression of the calcium-binding proteins. *Anat Rec*, 00:000–000, 2014. © 2014 Wiley Periodicals, Inc.

---

Grant sponsor: National Science Foundation; Grant number: BCS-0827531; Grant sponsor: James S. McDonnell Foundation; Grant numbers: 220020293, 22002078; Grant sponsor: ONR; Grant number: N000141210731; Grant sponsor: NIH; Grant number: 5-R01DC011808.

\*Correspondence to: Joan S. Baizer, Ph.D., University at Buffalo, Physiology and Biophysics, 123 Sherman Hall, SMBS, Buffalo, New York. E-mail: baizer@buffalo.edu

Received 10 August 2013; Accepted 9 June 2014.

DOI 10.1002/ar.23000

Published online 00 Month 2014 in Wiley Online Library (wileyonlinelibrary.com).

**Key words: tinnitus; auditory system; brainstem; hair cells; cochlea**

## INTRODUCTION

The cochlear nuclear complex, the dorsal and ventral cochlear nuclei (DCN and VCN), receives input from the eighth cranial nerve. The anatomy and physiology of the DCN have been studied in many species including the mustached bat, baboon, cat, chinchilla, gerbil, guinea pig, hamster, monkey, mouse, rabbit, rat, and opossum, (representative papers include Osen, 1969; Disterhoft et al., 1980; Mugnaini et al., 1980b; Zook and Casseday, 1982; Wouterlood et al., 1984; Hackney et al., 1990; Fleckeisen et al., 1991; Ryugo et al., 1995; Moore et al., 1996; Bazwinsky et al., 2008; Rubio et al., 2008; Zhang and Guan, 2008). Two features of DCN organization are described for all nonhuman species. First, the DCN has a laminar organization, typically described as three layers. In the outermost, molecular layer (layer 1), there are few neuronal somata and many dendrites of neurons whose somata are in layer 2. Layer 1 also includes the parallel fibers, which are the axons of granule cells. The second layer (2), the fusiform/pyramidal/granule layer, contains the somata of the large projection neurons. The third layer, the deep or polymorphic layer, has an assortment of cell types. Deep to the DCN are the fibers of the dorsal acoustic stria (das), comprised of the axons of the DCN projection neurons as well as other fibers from multiple brain regions projecting to the DCN (Barnes et al., 1943; Gacek, 1973; Adams and Warr, 1976; Masterton and Granger, 1988; Cant and Benson, 2003; Smith et al., 2005).

The second major characteristic of DCN organization is the existence of distinct neuronal types with predictable synaptic relations to each other. Cataloging the different morphological types of neurons in the DCN was a major concern of early neuroanatomists (Lorente de Nó, 1933; Ramón y Cajal, 1953; Lorente de Nó, 1981) who used Golgi and Nissl stains. Many subsequent studies have supplemented these observations with additional techniques including immunohistochemistry (IHC) and electrophysiology coupled with intracellular filling of neurons (Zhang and Oertel, 1993a,b,c). Oertel and Young (2004) summarized these results and showed seven identifiable DCN neuron types and their interconnections. There are two classes of excitatory projection neurons, the pyramidal/fusiform cells and the giant cells, two classes of local excitatory cells, the granule cells and the unipolar brush cells (UBCs), and four kinds of inhibitory interneurons, cartwheel cells, stellate cells, Golgi cells, and tuberculoventral cells. An additional rare type of neuron not included in the review of Oertel and Young (2004) are the Purkinje-like cells (Spatz, 1997, 2003).

Studies of the human DCN have suggested there are fewer layers and fewer cell types than in other mammals (Moore and Osen, 1979; Moore, 1980; Heiman-Patterson and Strominger, 1985; Adams, 1986; Wagoner and Kulesza, 2009). Studies disagree, however, about how

many layers and how many cell types are in fact present in the human DCN. Cajal noted that the DCN was “poorly developed in humans—much more differentiated in other mammals such as the guinea pig, rabbit, and cat.” Adams (1986) described the human DCN as composed of “hypertrophied versions” of layers 3 and 4. Moore and Osen (1979) described the human DCN as missing a molecular layer, with only layers analogous to layers 2 and 3 of other animals. Heiman-Patterson and Strominger (1985) stated that “the laminar pattern [of the DCN] becomes progressively obscured” in higher primates. Wagoner and Kulesza (2009) recognized three layers, a molecular layer, a granule cell layer and a “deep” layer. They did describe a population of large cells but noted that these were found in clusters and not in a single row. By contrast, Adams (1986) suggested that fusiform neurons were absent from the human DCN, and Heiman-Patterson and Strominger (1985) emphasized the granule cell population was greatly reduced in humans.

We have reexamined the laminar and cellular organization of the human DCN using immunohistochemistry to supplement Nissl staining. We immunostained sections from cases from the Witelson Normal Brain Collection (Witelson and McCulloch, 1991); we previously described immunostaining in other brainstem structures in these cases (Baizer et al., 2007; Baizer and Broussard, 2010; Baizer et al., 2011a,c). In those earlier studies we found that analysis of the expression of several proteins including nonphosphorylated neurofilament protein (NPNFP), the synthetic enzymes for GABA and nitric oxide, and three calcium-binding proteins were especially useful in staining neurons and structures in the vestibular and precerebellar brainstem. We found them equally useful for visualizing the laminar organization and neurons in the human DCN. In order to compare the neurochemical properties of the human DCN to the DCN in other species, we used the same antibodies and immunohistochemistry methods on DCN sections from the macaque monkey, the cat, and three rodents, (the rat, the chinchilla, and the guinea pig).

Our results for humans demonstrate laminar organization of the DCN, but with only two layers, and several neurochemically identified cell types including NPNFP-immunoreactive (ir) projection neurons. However, we also found major differences among species in the neuronal characterization with the different markers. Some of these findings have been described in two abstracts and a short report (Baizer et al., 2012a,b; Baizer et al., 2013a).

## EXPERIMENTAL PROCEDURES

### Tissue Preparation: Humans

We studied eight human brainstems from the Witelson Normal Brain Collection (Witelson and McCulloch,

**TABLE 1. The human cases; DCN analysis**

Case	Gender	Age	PMI (hr)	Cause of death	DCN mm	CV sections	IHC sections	Total
155	F	50	9	Breast cancer	2.8	2	13	15
158	M	51	1	Colorectal cancer	4.6	19	32	51
164	F	45	3	Breast cancer	2.2	7	18	25
166	F	65	3	Breast cancer	2.6	6	22	28
168	M	69	3	Rectal cancer	2.4	7	25	32
169	M	70	2	Colorectal cancer	2.4	7	25	32
176	F	71	3	Colon cancer	2.8	3	17	20
180	M	54	2	Adenocarcinoma	3.4	3	19	22

**TABLE 2. Antibodies and dilutions**

Antigen	Source	Species/type	Catalogue #	Dilution
Calbindin (CB)	Chemicon	Rb, polyclonal	AB1778	1:1,000–1:2,500
Calretinin (CR)	Chemicon	Rb, polyclonal	AB5054	1:1,000–1:3,000
Eps8	BD Transduction Laboratories	Ms, monoclonal	610143	1:500
GAD65/67	Chemicon	Rb, polyclonal	AB1511	1:1,000–1:2,000
NPNFP	Covance	Ms, monoclonal	SMI32	1:1,000–1:2,000
Parvalbumin (PV)	Millipore	Rb, polyclonal	AB9312	1:2,000
nitric oxide synthase (nNOS)	Cayman	Rb, polyclonal	160870	1:250

1991). The critical parameters for these cases are summarized in Table 1. The brains had been stored in 10% formalin. They were cryoprotected in 15% and then 30% sucrose in 10% formalin. We cut 40  $\mu\text{m}$ -thick frozen sections on an American Optical (AO) sliding microtome equipped with a custom-built freezing stage. The brainstems were cut in a plane transverse to the long axis of the brainstem, the plane used in the atlas of Olszewski and Baxter (1954). All sections were saved and collected in 5% formalin in large, plastic compartment boxes, 5 sections/compartment, 36 compartments/box. They were stored in a cold room at 4°C. Initially, for each case, sets of sections about 1 mm apart through the brainstem had been mounted on gelatin-coated glass slides and stained with cresyl violet (CV; LaBossiere and Glickstein, 1976). We used these sections for localization of brainstem structures by comparing the appearance of the brainstem on our sections to the sections shown in atlases of the human brainstem (Olszewski and Baxter, 1954; Paxinos and Huang, 1995). In the course of these projects additional sections were mounted and stained for CV as needed to define more precisely the borders of structures of interest.

### Immunohistochemistry: Human Tissue

Sections selected for immunohistochemistry, were first processed with an antigen retrieval protocol. Sections were removed from the formalin, rinsed in 0.1 M phosphate buffered saline (PBS; all rinses were  $3 \times 10$  min on a tissue rocker) and placed individually in glass jars in 20 mL of a sodium citrate-citric acid buffer, pH adjusted to 2.8, 6.0, or 8.0. The jars were placed in a water bath preheated to 85°C for 20–30 min, then cooled at room temperature for 20 min. The sections were removed from the jars and rinsed in PBS. Nonspecific antibody binding was blocked by incubating the sections in a solution of PBS, 1.5% normal serum (NS) from the species in which the secondary antibody was made (Vector Laboratories, Vector Elite kits, Burlingame, CA) and

2% TritonX-100 (Sigma-Aldrich, Saint Louis, MO). Sections were then incubated overnight on a tissue rocker at 4°C with the primary antibody (added to the blocking solution). Table 2 shows the primary antibodies and dilutions used. Subsequent processing was with the appropriate Vector ABC Elite kit (anti-mouse or anti-rabbit IgG biotinylated secondary antibodies) for 1 hr at room temperature on a rocker, followed by  $3 \times 10$  min rinses in PBS. Sections were then incubated with the avidin-biotin complex, ABC, for 1 hr according to manufacturer's instructions and rinsed again prior to the visualization step. We used two different visualization protocols. The first was a standard DAB protocol. Immunoreactivity was visualized by incubating in 3,3'-diaminobenzidine (DAB, Sigma) with 0.0015–0.003%  $\text{H}_2\text{O}_2$  in 0.01 M PBS. For other sections, immunoreactivity was visualized by the glucose oxidase modification of the DAB procedure (Shu et al., 1988). We found that the glucose oxidase procedure allowed better visualization of fibers than the standard DAB procedure. Sections were then mounted on gelatin-coated glass slides, air-dried, dehydrated in graded concentrations of alcohols, cleared in Histosol (National Diagnostics) or xylene and coverslipped with Permount (Fisher Scientific, Pittsburgh, PA).

### Antibody Characterization and Specificity

Antibody specific and controls for several of these antibodies in human tissue were previously described (Baizer and Broussard, 2010; Baizer et al., 2011b).

### Calbindin

The immunogen was recombinant rat calbindin. The calbindin D28 antiserum (AB1778) was affinity purified and preadsorbed against calretinin. It recognizes a band of 28 kDa on a Western Blots of mouse brain (manufacturer's data sheet). No immunostaining was seen on control sections on which the primary antiserum was omitted or on sections in which the antiserum was

diluted (1 : 2,000) and incubated with the protein (Swant, recombinant rat calbindin, 2 µg/mL, in 1 mL antibody diluent) for 6 hr at 4°C prior to immunostaining (following the Swant protocol) (Baizer and Broussard, 2010).

### Calretinin

The immunogen was recombinant rat calretinin. The calretinin antiserum (AB5054) recognizes a band of 31 kDa on Western Blot of rat brain (manufacturer's data sheet). It recognizes both the calcium-bound and calcium-unbound conformations of calretinin by western blots (data from manufacturer). No immunostaining was seen on control sections of the human brainstem in which the antiserum was omitted or in sections in which the antiserum was diluted (1 : 1,500 in 1.5 mL of antibody diluent) and preincubated with the calretinin protein (Swant, recombinant human calretinin produced in *E. Coli*, 3 µg/mL) for 6 h at 4°C prior to immunostaining (following Swant instructions) (Baizer and Broussard, 2010). It has also been used to label neurons in mouse thalamus (Delaunay et al., 2009) and interneurons in mouse cerebral cortex (Liodis et al., 2007). This antibody also showed the predicted labeling of hair cells in the chicken (Warchol and Speck, 2007), of interneurons in the rat striatum (Yang et al., 2008), and neurons in the rat amygdala (Rainnie et al., 2006).

### Eps8

The immunogen was mouse Eps8, aa 628–681. The Eps8 antiserum (61043) recognized a band at 97 kDa on a Western Blot of mouse macrophage lysate (manufacturer's data sheet). In the study establishing Eps8 as a UBC marker in rats, there was no immunostaining in control sections incubated without the primary antibody (Sekerikova et al., 2007).

### GAD65/67

The immunogen was a synthetic peptide with the amino acid sequence [C]DFLIEEIERLGQDL from rat glutamate decarboxylase (GAD65; C-terminus residues [Cys]+572–585). The GAD 65/67 antiserum (AB1511) recognizes a doublet on Western Blot of mouse brain lysates at 65/68 kDa (manufacturer's data sheet). Immunostaining was abolished by preincubation with the peptide (manufacturer's data sheet). This antibody has previously been used for immunohistochemistry in rat brainstem (Belenky et al., 2008; Yeo et al., 2010) and in mouse cerebral cortex (Liguz-Leczna et al., 2009).

### nNOS

The immunogen was human nNOS, aa 1422–1433. The nNOS antiserum (160870) recognizes a peptide of 155 kDa on Western blot of mouse brain (manufacturer's quality control sheet). In human sections, no immunostaining was seen on control sections in which the antiserum was omitted, or on sections in which the antibody was first incubated with the immunizing protein (Cayman Laboratories Catalogue 360871, 1 µg/ml) for 1 hr at RT prior to dilution (1:200 in 2 ml of antibody diluent; following Cayman instructions) (Baizer and Broussard,

2010). This antibody was also used to identify neurons in the hippocampus of the rat (Armstrong et al., 2011).

### NPFP

The immunogen was rat brain lysate. The antiserum (SMI32) recognizes a nonphosphorylated epitope on the 168 (M, medium) and 200 kDa (H, heavy) neurofilament subunits (Sternberger and Sternberger, 1983) of most mammalian species, and stains somas, dendrites and some thick axons (manufacturer's data sheet). It lacks cross reactivity to microtubule-associated protein and to Alzheimer's disease neurofibrillary tangles (Ksiezak-Reding et al., 1987; Lee et al., 1988). It has been widely used to characterize cortical pyramidal cells in several species (Hof and Morrison, 1990; Hof et al., 1995; Van der Gucht et al., 2007).

### Parvalbumin

The immunogen was rat muscle parvalbumin. The antiserum (AB9312) recognizes both the calcium bound and calcium-free forms of parvalbumin. The specificity of this antibody for parvalbumin in the rodent brain was described by Felch and Van Hooser (2012). It was also shown to label neurons in cortex of rat and mouse (Salgado et al., 2007; Schmid et al., 2008) and also used in a study of cortical dysplasia in humans (André et al., 2008).

### Tissue Preparation: Nonhuman Specimens

Our goal was to compare the immunostaining in the human DCN other species. We utilized tissue from several different sources, but the immunohistochemistry was done in this laboratory with the same antibodies used for the human tissue. All animals had been perfused with fixative (10% formalin or 4% paraformaldehyde, PFA). All animal experiments had been conducted according to the NIH guidelines and had been approved by the Animal Care and Use Committees of the institutions in which they were done.

### Macaque Monkeys

We illustrate sections from the brains of three different adult macaque monkeys.

**Macaque A.** We examined archival CV-stained sections from this animal. The animal had been perfused with 10% formalin and the brain removed and stored in 10% formalin. The brain was cryoprotected in sucrose in formalin, divided into two blocks and cut at 40 µm in the coronal plane. Every section was collected and stored at –20°C in a cryoprotection-storage solution (30% ethylene glycol, 30% glycerol in 0.1 M PB). Sections used for IHC were pretreated with an antigen retrieval protocol as for the human tissue.

**Macaque B.** We had available some archival immunostained sections from this monkey. The animal had been perfused with 4% PFA followed by 0.1 M PBS. The brain was divided into two blocks in the frontal plane at about stereotaxic A13 (Paxinos et al. 2000). For cryoprotection, tissue blocks were immersed in 15% then 30% sucrose in PBS. They were then stored in an –80°C

freezer in a different cryoprotection solution of 30% ethylene glycol and 30% glycerol in 0.1 M PB. Subsequently, 50  $\mu\text{m}$ -thick frozen sections were cut on a sliding microtome. The sections were stored in the glycerol-ethylene glycol cryoprotectant solution in tissue culture plates at  $-20^{\circ}\text{C}$  until processing. Data from this animal were included in earlier reports on different brainstem structures (Baizer and Baker, 2006a,b; Baizer et al., 2011c).

***Macaque C.*** This macaque monkey had been perfused with 4% PFA and the brain stored in PBS with 0.1% sodium azide. A block of tissue containing the brainstem and cerebellum was sent to this laboratory, cryoprotected in 15% then 30% sucrose in PBS and then frozen sections cut on the AO sliding microtome in the coronal plane at 40  $\mu\text{m}$ . All sections were collected and stored in plastic compartment boxes in a cryoprotection solution (30% ethylene glycol and 30% glycerol in 0.1 M phosphate buffer) in a  $-20^{\circ}\text{C}$  freezer. Data from this animal were included in an earlier report (Baizer et al., 2013b).

***Cats.*** We immunostained DCN sections from 5 adult cats. The brains had been prepared for projects on the vestibular nuclear complex (VNC) and related nuclei (Baizer and Baker, 2005, 2006b; Baizer et al., 2010). The animals had been perfused with 4% PFA and the cerebella dissected free from the brainstems. The brainstems were cryoprotected in 15% then 30% sucrose in PBS. Frozen sections, 40  $\mu\text{m}$ -thick, were cut in the coronal/frontal plane on the AO sliding microtome. This plane of section was illustrated in an atlas of the cat brainstem (Berman, 1968). All sections were collected and were stored in a cryoprotective storage solution (30% ethylene glycol and 30% glycerol in 0.1 M PB) at  $-20^{\circ}\text{C}$ . Since the DCN is present at the same rostro-caudal levels as components of the VNC, some sections at the level of the DCN had been used for other projects. We also examined archival celloidin-embedded coronal Nissl- and fiber (Weil)-stained sections of cat and monkey brains.

***Chinchilla.*** We used sections from the brain of an adult chinchilla that had been perfused with 4% PFA; sections were used for pilot experiments extending a different project (Manohar et al., 2012). The brain was cryoprotected in 15% then 30% sucrose in PBS and frozen sections were cut on the AO sliding microtome at 40  $\mu\text{m}$  in the coronal plane. Sections had been stored in cryoprotection solution; some sections had been stained with CV or used for immunostaining. We also examined archival CV and immunostained sections of two additional chinchillas.

***Rats.*** We used sections from the brains of three rats (2–4 months) that were prepared in the context of other projects (Manohar et al., 2012; Paolone et al., 2014). Those animals had been perfused with 4% PFA, the brains postfixed overnight and cryoprotected in 15% then 30% sucrose in PBS. The brains had been sectioned in the coronal plane at 40  $\mu\text{m}$  on a cryostat and the sections stored at  $-20^{\circ}\text{C}$  in a cryoprotection solution (30% ethylene glycol, 30% glycerol in 0.1 M PB).

***Guinea pigs.*** We studied the brains of two adult guinea pigs that had been perfused with 4% PFA, cryo-

protected in 15% and then 30% sucrose in PBS, and sectioned in the coronal plane at 40  $\mu\text{m}$ . The sections were stored in a  $-20^{\circ}\text{C}$  freezer in a cryoprotection solution (30% glycerol, 30% ethylene glycol in PB).

We used the same antibodies and immunohistochemistry protocols for these species as for the humans. The protocols were modified in that we omitted the antigen retrieval protocol (since the tissue had not been stored in fixative) and the Triton-X100 concentration was decreased from 2% to 0.5%.

We also used a double-labeling immunofluorescence protocol with sequential incubations for a few macaque monkey sections (Macaque C). The sections were incubated overnight with the first primary antibody. They were rinsed, incubated with the appropriate Alexa fluorescent secondary antibody (Alexa anti-mouse 488 or Alexa anti-rabbit 594), rinsed, incubated overnight with the second antibody and the next day with the appropriate secondary antibody. Immunofluorescence slides were coverslipped with Vector Hardmount mounting medium and examined with a Zeiss Axioimager microscope. Digital images were captured with Zeiss AxioVision software and exported as .tif files.

## Data Analysis and Photography

The DAB and DAB-GO sections were examined with a Leitz Dialux 20 light microscope, and digital images (1,200  $\times$  1,600 pixels) captured with a SPOT Insight Color Mosaic camera mounted on that microscope. Brightness and contrast of images were adjusted with Adobe Photoshop, (San Jose, CA), and plates assembled using Adobe Photoshop. For ease of comparison, all DCN images are shown as on the right. We used a screenshot of one image of the cat DCN in a parasagittal section from Brainmaps.org, cat parasagittal series, section #579 (inset in Fig. 6A). That image was cropped, and brightness, contrast, and color adjusted in Adobe Photoshop.

## RESULTS

Our goal was to examine the organization of the human DCN using immunohistochemistry for proteins that we knew are expressed in other structures in the human brainstem. We found that IHC for several markers showed a characteristic and consistent staining pattern in the human DCN, revealing details of laminar organization and neuronal types not previously described. We then compared the neurochemical organization of the human DCN with that of other species using the same panel of markers. We will first describe the results in the human and then compare the human DCN with the macaque monkey, cat and rodents. For each species, we will first describe the appearance of the DCN in Nissl-stained sections and then the laminar and cellular organization as shown by IHC.

### Human DCN

For each case, we first used the CV and immunostained sections to determine the rostro-caudal extent of the DCN. Table 1 shows the total number of sections analyzed for each case and the rostro-caudal extent of

the DCN. There is some variability among cases in the DCN extent.

**CV.** Figure 1 shows low (A, C, E) and high (B, D, F) magnification images of CV-stained sections of the human DCN from three different cases. In Cases 158 (Fig. 1A) and 168 (Fig. 1E) only the DCN is present, in Case 180 (Fig. 1C) the ventral cochlear nucleus (VCN) is present as well. The shape and thickness of the DCN vary among cases, but in all three cases it is possible to identify an outer region (labeled 1) with lighter staining and only a few stained somata, and deep to that a broader region (labeled 2) with numerous scattered stained somata. In these sections, the borders between the DCN, the das and the underlying inferior cerebellar peduncle (icp) are not sharply delineated. For the descriptions of the laminar organization of the human DCN we will use the term “band” rather than “layer” to avoid implied homology with the layers of the DCN established in other species. The panels on the right show the scattered large, stained somata. The shapes of the somata vary from fusiform (Fig. 1B, arrows) to shield-shaped (Fig. 1D, arrow) to oval (Fig. 1F, arrow). These large neurons are not arranged in a single row but scattered over the width of band 2. Furthermore, the elongated or spindle-shaped somata are not aligned with their long axes perpendicular to the surface of the DCN.

**NPNFP.** The appearance of the DCN in CV staining is only faintly suggestive of laminar organization. By contrast, NPNFP-immunoreactivity clearly revealed a laminar organization. Figure 2A shows NPNFP staining in the DCN of one human case. At low magnification, three distinct bands of staining of different intensities can be seen. There is an outer, lightly stained narrow band (1), a broad inner darkly stained band (2) and deep to that another lightly stained narrow band (3) which corresponds to the das. The border between the das/DCN and the underlying icp is clear. The inset shows an adjacent section stained with CV. This section is adjacent to the CV-stained section shown in Fig. 1A,B. Figure 2B shows that the broad middle band (2) consists of stained somata embedded in a dense meshwork of stained processes, most of which are oriented parallel to the surface of the DCN. The deepest band includes stained processes running parallel to the surface of the structure (example at arrowhead). Figure 2C shows a higher magnification image of band 1 and the outermost portion of band 2. There is a stained neuron (arrowhead) in band 1, but in general stained somata are sparse, especially compared to band 2. There are also some stained processes parallel to the DCN surface. Figure 2C also shows stained elongated (fusiform; example at arrow) somata in the outer part of band 2. The somata of fusiform cells are seen at all different orientations and their processes do not routinely enter band 1. Figure 2D shows that deeper band 2 also contains stained somata of a number of different shapes (round soma shown at arrow) and again a very dense network of stained processes running at all different orientations.

**Nitric oxide synthase (nNOS).** Staining for nNOS similarly shows a laminar organization of the human DCN with many of the same features as seen

with NPNFP immunostaining. Figure 3A shows a low magnification image of nNOS immunostaining with a lightly stained, narrow, outer band, a broad and darkly stained middle band (band 2) and a lightly stained inner band around the icp. Figure 3B is a higher magnification image to illustrate the staining in the three bands. The middle band contains many stained somata but their distribution is not as homogeneous as seen with NPNFP immunostaining. nNOS-ir somata are distributed more densely in the inner part of band 2 than in the outer part. The background staining is punctate and the stained meshwork of fibers seen with NPNFP is not apparent. There are occasional large stained somata deep to band 2 (Fig. 3B, arrowheads) as well as stained processes. Figure 3C shows a variety of immunostained soma shapes and sizes in band 2 and Figure 3D shows a rare stained neuron in the outer band (1).

**Calretinin (CR).** Figure 3E shows that staining for CR also suggests a laminar organization with the same three distinct bands of staining, an outer (1) lightly stained band, a broad middle band (2) and a more lightly stained inner band (3). However, the higher magnification images in F, G, and H show that different elements are better immunostained with CR than with either NPNFP or nNOS. Figure 3F shows scattered small round (example at arrow) or oval somata scattered in the broad middle band; similar profiles were not seen with the other two stains. There are also long stained fibers running parallel to the outer edge of the DCN (arrowhead). Figure 3G shows the diversity in CR-ir somata, with very small round (arrow) and slightly larger profiles labeled, suggesting that more than one neuronal type expresses CR. The CR-ir neurons, like the nNOS-ir neurons, tended to be located in the ventral half of band 2. Finally, Fig. 3H (arrowhead) shows that in the deepest band (3) there are stained fibers running along the length of the DCN.

**Calbindin (CB).** The staining with CB also showed a laminar pattern with a lightly stained outer band (Fig. 3I) and a more darkly stained, broader band (2). In the outer band a few beaded stained processes are seen (Fig. 3I, black and white arrowheads; Fig. 3J, white arrowhead). The middle band contained a few scattered stained elements. There were also stained fascicles of fibers; Figure 3J shows two such fascicles (arrow) deep in band 1 of another case. In a few sections, there is also dramatic staining of very large neurons (Fig. 3K,L), that are similar to the “Purkinje-like cells” previously described in the DCN of other species (Spatz, 1997, 2003).

**Glutamic acid decarboxylase (GAD).** Figure 4A shows dark and uniform GAD immunostaining in the outer two layers of the DCN. The higher magnification image in 4B shows that this staining consists of puncta with a few stained somata. The image in 4C shows examples of stained somata in band 1 (arrow). Figure 4D shows the pattern of GAD staining in the human cerebellar cortex, with stained fibers in the molecular layer (white arrowhead), and staining of Purkinje cells (P) and their dendritic trees. In the granule cell layer (gr) many round somata are outlined with punctate staining

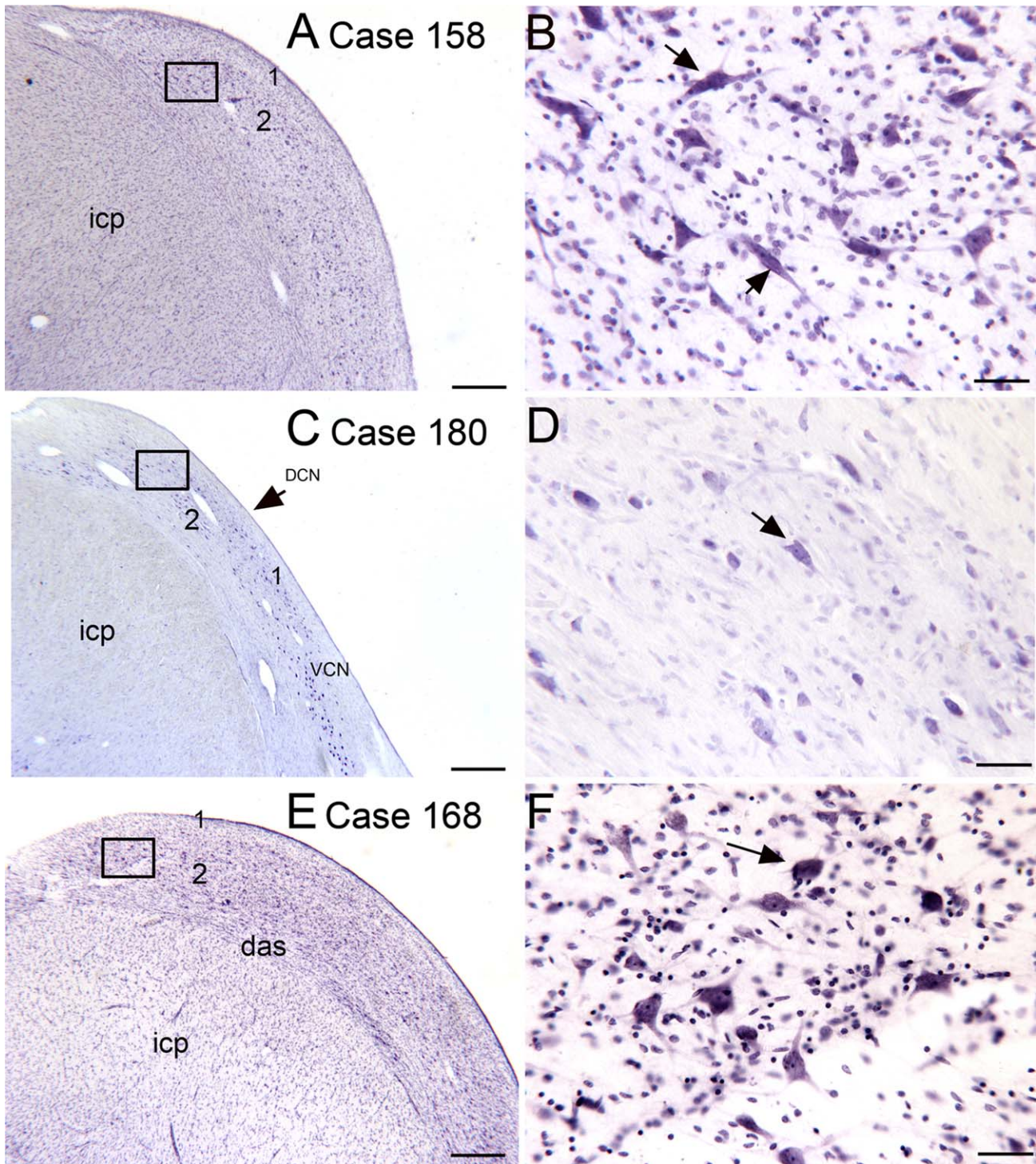


Fig. 1. Cytoarchitectural appearance of the human DCN in three different cases, CV staining. Two images are shown for each case, a lower magnification image on the left (**A, C, E**) and a higher magnification image on the right (**B, D, F**). A rectangle on the left panel outlines the region shown in higher magnification. The arrows indicate neurons. The

number 1 in **A, C, E** indicates the outer band with few somata and the number 2 indicates the deeper band that includes the stained somata shown in **B, D, F**. CV, cresyl violet; das, dorsal acoustic stria; DCN, dorsal cochlear nucleus; icp, inferior cerebellar peduncle; VCN, ventral cochlear nucleus. Scale bars: **A, C, E** = 500  $\mu$ m; **B, D, F** = 50  $\mu$ m.

(example at arrow). Figure 4E shows a lower power image of the DCN in another case; a lightly stained outer band and a darkly stained band 2 are clear. The

image in panel 4F again confirms that the GAD stains puncta and does not distinguish very many somata. The border between bands 1 and 2 is clear.

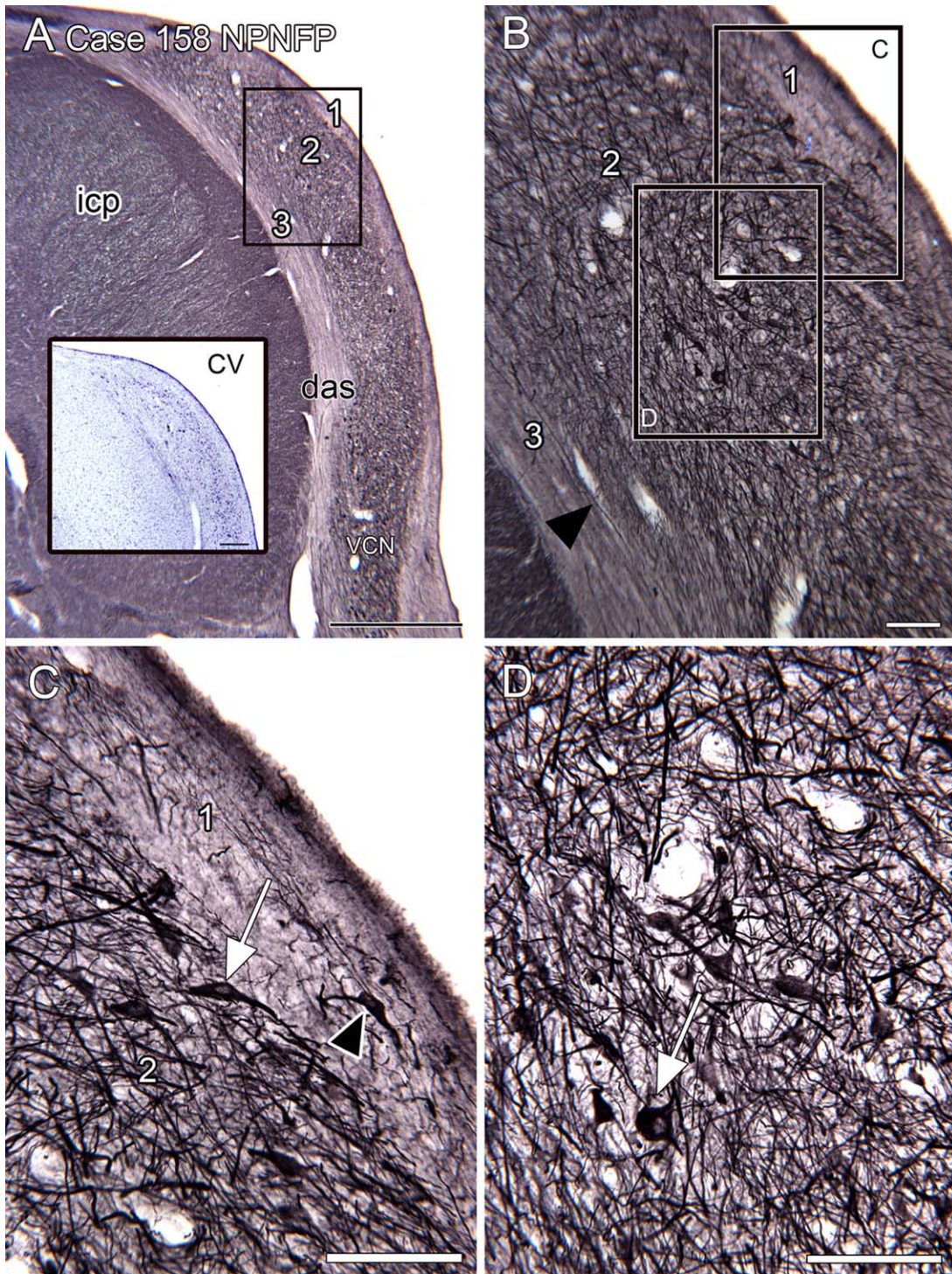


Fig. 2. NPNFP immunostaining in the human DCN. **A:** NPNFP shows three distinct bands (1, 2, and 3). The laminar pattern is not as clear on an adjacent section stained for CV (inset). The rectangle shows the location of the image in B. **B:** The outer band (1) contains a few stained processes and somata. Band 2 is broader and is comprised of many stained somata and processes. In the innermost band (3) there are stained fibers running parallel to the border with the icp

(example at arrowhead). The rectangles show the locations of the images in C and D. **C:** The arrowhead indicates a stained soma in band 1; the arrow indicates a neuron with an elongated soma at the outer border of band 2. **D:** The arrow shows a stained soma embedded in a dense meshwork of stained processes. icp, inferior cerebellar peduncle; VCN, ventral cochlear nucleus. Scale bars: A = 1 mm; inset = 500  $\mu$ m; B, C, D = 100  $\mu$ m.

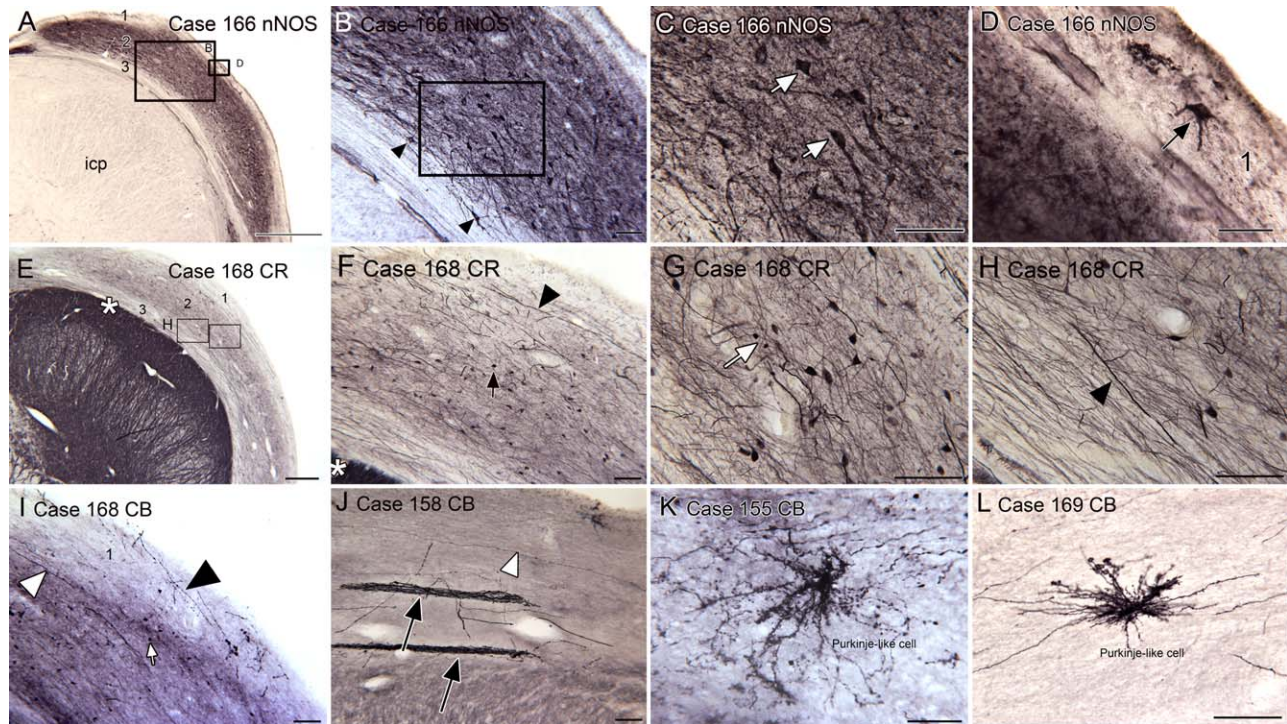


Fig. 3. nNOS, CR, and CB immunoreactivity in the human DCN. **A:** nNOS. The rectangles show the locations of the images in panels B, C. **B:** nNOS immunostaining. Labeled somata are scattered in band 2 with larger neurons deeper in the band. The rectangle shows the location of the image in C. There are a few stained somata (arrowheads) deep to 2. **C:** Labeled somata in band 2 are of different shapes from oval to multipolar (examples at arrows). **D:** The arrow shows a large stained soma in the outermost band (1). **E:** CR. Low magnification image of the DCN showing that CR immunoreactivity defines an outer narrow lightly stained band (1), a broad middle band (2) and a lightly stained, narrow, inner band (3). The asterisk is an alignment point for the image in F. The rectangles show the locations of the images in G and H. **F:** There are long stained processes in the outer band that run parallel to the surface

of the DCN (example at arrowhead). In band 2 there are scattered stained small somata (example at arrow) and stained processes. **G:** Higher magnification image of the stained somata (examples at arrow) in band 2. **H:** The deepest band (3) includes stained processes (example at arrowhead). **I:** CB immunostaining shows a lightly stained outer band (1) with a few fine beaded fibers (example at arrowhead) running parallel to the pial surface. Below that is a more darkly stained band (2) with small stained profiles (example at arrow) and stained processes running parallel to the surface (example at arrowhead). **J:** In band 1 there are two fascicles of CB-ir fibers (black arrows) and a long, thin beaded process (white arrowhead) all running parallel to the surface. **K:** CB-ir Purkinje-like cell. **L:** CB-ir Purkinje-like cell from a second case. Scale bars: A = 1 mm; B, C, F, G, H, I, J, L = 100  $\mu$ m; D, K = 50  $\mu$ m; E = 500  $\mu$ m.

**Parvalbumin (PV).** Staining for the third calcium-binding protein, PV, again confirms laminar organization in the human DCN. Figure 4G shows a lower magnification image of PV-ir in the DCN. This section is adjacent to the section shown in Fig. 1C. Again, three different bands are seen with PV immunostaining, an outer lightly stained band, a broad more darkly stained middle band (2) and a deep band (3) that is very darkly stained, a pattern different from what is seen with the other calcium-binding proteins. The higher magnification image shows that the staining in all layers consists of fibers running along the DCN (Fig. 4H, arrow and arrowhead). There are a few fibers with varicosities (Fig. 4H, arrowheads). There is no staining of cell bodies in any layer.

### Macaque Monkey

Figure 5A shows a CV-stained section through the DCN. CV staining clearly shows a laminar organization in the macaque DCN that is similar to the classical picture of laminar organization based on cat and rodent. There is an outer layer (1) with few stained somata. Under that is a band of large, darkly stained neurons

(arrow), and deep to that a region of scattered stained somata. Under the cellular layers are the fibers of the das. The inset shows a CV-stained section from a more rostral level showing a region of stained small neurons, the granule cell domain (GCD; Fig. 5A inset, arrow).

### Immunohistochemistry

The staining with NPNFP shows a laminar organization similar to the pattern in human. Figure 5B shows a lightly stained outer layer (1) and a broad band of staining beneath. That band consists of staining of both somata and processes, with the stained somata deeper in the band (Fig. 5B, arrowhead indicates the level of the stained somata). Deep to the DCN a few stained processes are seen in the das (Fig. 5B, arrow). The higher magnification image shows round or oval somata (Fig. 5C, arrow). The laminar pattern with nNOS is different from in the human. Instead of a lightly stained band 1 there is an outer region of darker staining (Fig. 5D). As in human, nNOS labels scattered stained somata. These are elongated and oriented roughly parallel to the surface of the DCN (Fig. 5D,E). The inset in Fig. 5D shows

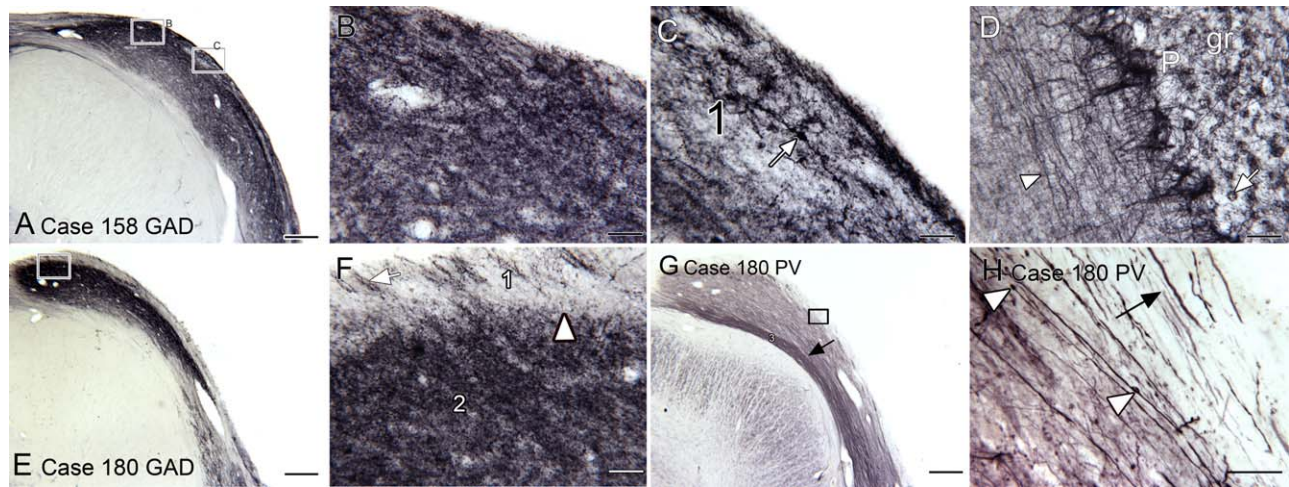


Fig. 4. GAD and PV immunoreactivity in the human DCN. **A:** Low magnification view of immunoreactivity for GAD in the DCN of Case 158 showing uniformly dark staining across the entire width of the DCN. The rectangles show the location of the images in B and C. **B:** The staining is fine and punctate. **C:** Staining of a soma (arrow) in the outer band (1). **D:** GAD in the cerebellar cortex. The arrowhead indicates a stained fiber. **E:** GAD staining in the DCN of another case. The rectangle shows the location of the image in F. **F:** Higher magnification showing the contrast in staining between bands 1 and 2. The arrow shows stained processes in band 1 running roughly perpendicular to

the surface. **G:** The same three bands are seen with PV staining, a narrow lightly stained outer band a broader middle band (2) and a narrow inner band (arrow) that with PV is more darkly stained. The rectangle shows the location of the image in H. **H:** At this magnification the lightly stained outer band is more apparent. There are stained processes (example at arrow) running parallel to the border of the DCN in this band. There are also stained processes running parallel to the surface in the middle band, some of which are beaded (examples at arrowheads). Scale bars: A, E, G = 500  $\mu$ m; B, C, D, F, H = 50  $\mu$ m. P, Purkinje cells; gr, granule cell layer.

a section that was double-labeled for nNOS and NPNFP. There are more NPNFP-ir cells (green, example at arrow) than nNOS-ir neurons (red, arrowhead). There were no examples of double-labeled neurons suggesting that these are different populations.

CR-immunoreactivity shows many stained small somata (example at Fig. 5F, arrow) and a few stained processes (Fig. 5F, arrowhead). The staining with CB is different from that in human, with a very few stained cells and profiles that appear to be dendrites (Fig. 5G,

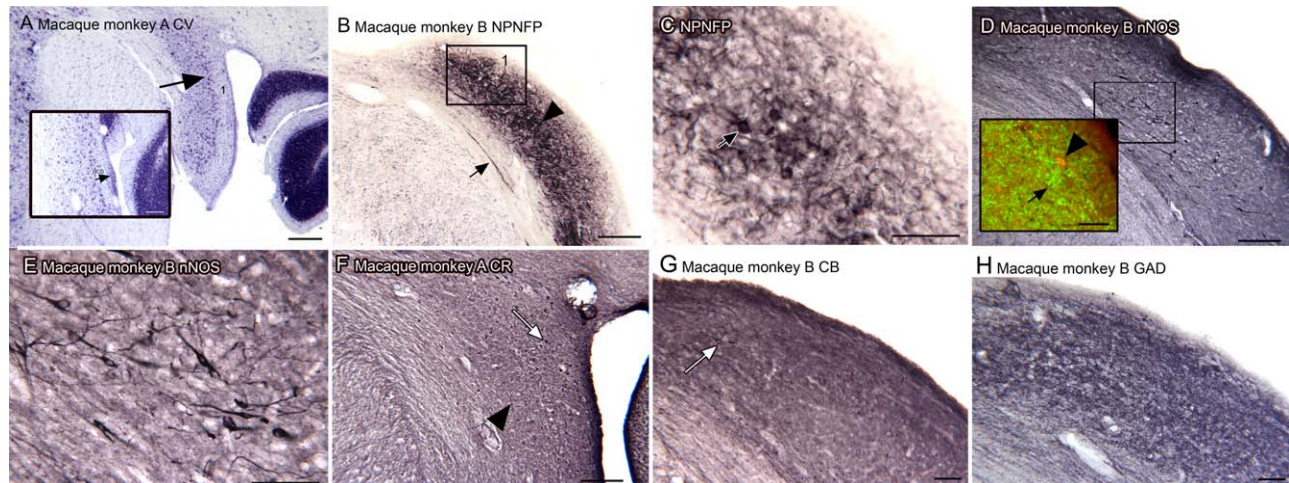


Fig. 5. The DCN in the macaque monkey. **A:** On a CV-stained section there is an outer, lightly stained layer (1) and a row of larger, darkly stained somata (arrow). Deep to that row is a broader region of scattered somata. The inset shows a more rostral CV-stained section showing a region of densely stained small somata (arrow), the granule cell domain (GCD). **B:** NPNFP immunoreactivity in the DCN shows a narrow lightly stained outer layer (1). The arrowhead marks the approximate boundary of a broad band of stained somata. The rectangle shows the location of the image in C. **C:** The NPNFP immunostained neurons have round or oval cell bodies (example at arrow). **D:**

nNOS immunostaining labels a few elongated somata and processes. The small rectangle shows the location of the image in E. The inset shows the DCN on a section double-labeled for nNOS (red) and NPNFP (green). The arrow shows a neuron that is NPNFP-ir and the arrowhead a neuron that is nNOS-ir. **E:** Elongated nNOS-ir somata. **F:** CR. Scattered CR-ir somata (example at arrow) and a few processes (arrowhead). **G:** There are occasional stained CB-ir elements that resemble stained processes (example at arrow). **H:** Punctate GAD staining. Scale bars: A = 500  $\mu$ m; B, D, F = 250  $\mu$ m; C, D- inset, E, G, H = 100  $\mu$ m.

arrow). Finally, GAD-ir (Fig. 5H) shows diffuse punctate staining throughout much of the depth of the DCN, a pattern similar to that of the human.

## Cat

The laminar organization of the DCN in the cat is easily apparent from CV-stained sections (Fig. 6A). There is an unstained outer layer (1), a darkly stained layer of somata (2), and a deeper region with scattered stained somata (3). The arrow indicates the GCD. The inset shows a parasagittal section of the cat DCN; the same laminar organization is apparent. Figure 6B shows the darkly stained large somata of layer 2 (arrow), and the scattered somata of a variety of shapes and sizes in layer 3 (elongated soma at arrowhead).

## Immunohistochemistry

In the cat, the immunostaining pattern for NPNFP is quite different from that seen in human or monkey. Figure 6C,D show that immunoreactivity for NPNFP stains an outer band along the perimeter of the DCN. This

region includes some stained cells and processes (Fig. 6D, arrow and arrowhead) and overlaps layers 1 and 2 shown in CV. While in human, the laminar pattern of nNOS immunostaining is similar to the staining with NPNFP, for the cat nNOS and NPNFP immunostaining are quite different. Figure 6E shows that nNOS defines a darkly stained outer band, narrower than the band defined by NPNFP staining. This band includes neurons with oval or round somata and processes (Fig. 6F); no such nNOS-ir neurons have been seen in human or monkey.

The immunostaining patterns for cat with the calcium-binding proteins are also different from those observed in human and monkey. CB immunostaining shows somata distributed throughout the cell layers of the DCN (Fig. 6G). The somata and proximal dendrites are stained; the somata are oval, round or elongated (Fig. 6H, arrow). CR stained scattered small round puncta and a few larger somata (Fig. 6I). Immunoreactivity to GAD marked a few somata in the cellular band (Fig. 6J, outlined arrow), small punctate staining and a few larger neurons intermingled with the fibers of the das (Fig. 6J, black arrowhead). Finally, PV (Fig. 6K,L)

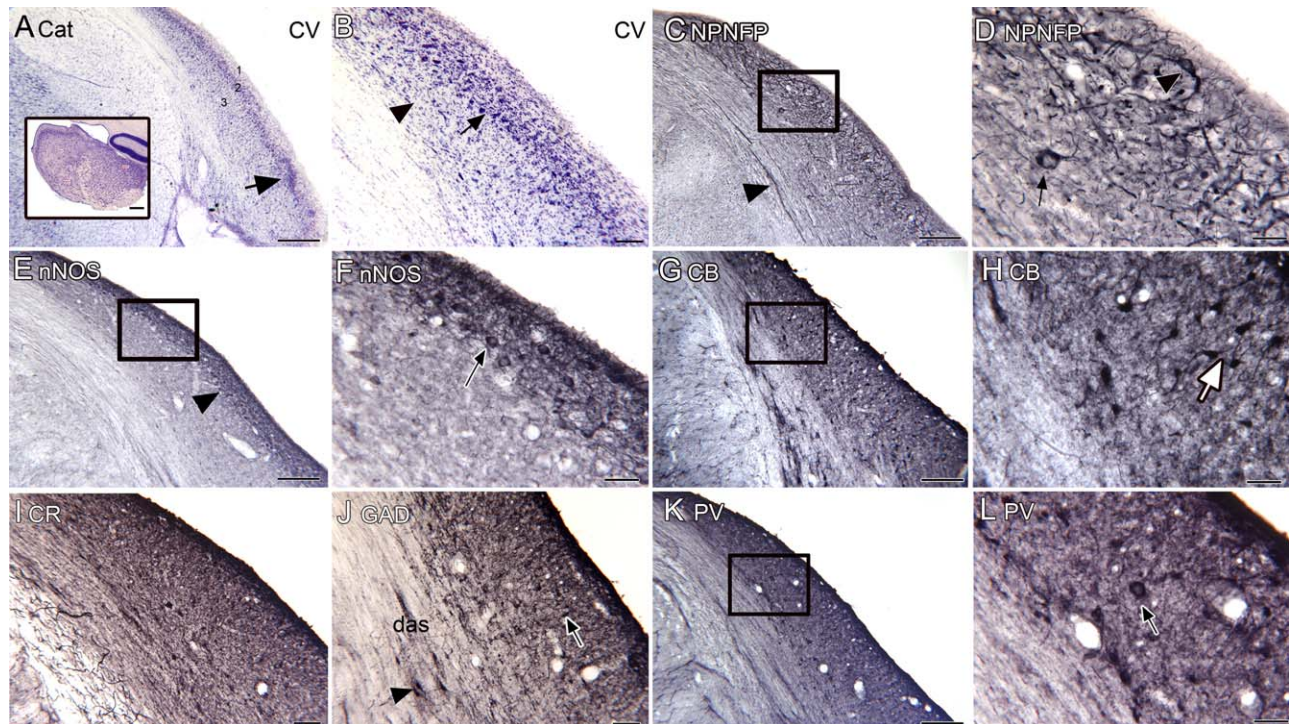


Fig. 6. The DCN of the cat. **A:** CV-stained coronal section through the cat DCN showing an outer, lightly stained molecular layer (1), a broad, darkly stained pyramidal cell layer (2) and a deeper layer (3) with scattered stained somata. The arrow marks a region of dense staining at the ventral edge of the DCN, the GCD. The inset shows the DCN in a parasagittal section (cropped screenshot of an image from the parasagittal atlas of the cat brain from brainmaps.org); the same laminar organization is apparent. **B:** Higher magnification image of the coronal section showing the large, darkly stained somata of a variety of shapes, (example at arrow) and large elongated somata in the deep layer (example at arrowhead). **C:** Low magnification image showing NPNFP staining in the outer half of the DCN. The rectangle shows the location of the image in **D**. **D:** Higher magnification image showing occasional stained somata (arrow and arrowhead) and fragments of

processes. **E:** nNOS in the cat DCN shows darker staining in an outer band of the DCN (arrowhead). The rectangle shows the image in **F**. **F:** There are nNOS-ir somata (arrow) in the outer band. **G:** CB staining shows a broad layer of scattered stained somata. The rectangle shows the location of the image in **H**. **H:** Stained round and elongated (example at arrow) somata and proximal dendrites. **I:** CR staining marks only a few stained profiles. **J:** With GAD-ir there are some stained small round profiles (example at arrow) and a few stained somata in the das (arrowhead). **K:** PV gives uniform light staining with a few stained somata. The rectangle shows the location of the image in **L**. **L:** There are occasional PV-ir large somata (arrow) in the deep layers. Scale bars A, C, E, G, K = 250  $\mu$ m; A, inset = 500  $\mu$ m; B, I, J = 100  $\mu$ m; D, F, H, L = 50  $\mu$ m.

immunostaining also marks stained somata (example at arrow, Fig. 6L). The immunostaining with the three calcium-binding proteins does not define the molecular layer as in human nor do they stain long processes running parallel to the DCN surface. Instead, they stain different populations of neurons.

## Rodents

**Laminar organization.** The appearance of the DCN in Nissl stains is different for each rodent, rat, chinchilla and guinea pig (Fig. 7). In rat, there is a lightly stained layer 1 (Fig. 7A,B). Beneath that are scattered, larger, darkly stained neurons (layer 2) and a very broad inner band with stained somata of a variety of shapes (layer 3). At this level, the VCN is present; between the DCN and the VCN is a region of darkly stained small neurons, the GCD; (Fig. 7A, arrowhead).

In the guinea pig, the DCN (Fig. 7C,D) is relatively larger and thicker than in the rat. However, the overall laminar organization is similar with a lightly stained layer 1 (Fig. 7C,D), ventral to that a more sharply defined layer 2 (Fig. 7D, arrow) and a broad layer 3 with scattered stained somata. The GCD is very well-defined (Fig. 7C, arrowhead).

The chinchilla DCN (Fig. 7E,F) is unique in that there is a patchy organization of layers 2 and 3. As in all species, there is a lightly stained outer layer (1) with very few stained somata (arrowhead in Fig. 7F). Medially there is a very densely stained patch of small neurons (Fig. 7E, leftmost arrow), an arrangement not seen in the other species. There is another cluster of neurons at the middle arrow (Fig. 7E) and, more ventrally, a third stained oval-shaped region (Fig. 7E, lateral arrow). The row of large cells in layer 2 is interrupted by the clusters of small cells. A broad layer 3 with a variety of soma sizes and shapes is also apparent (Fig. 7F, arrow indicates neuron with oval soma).

**Immunostaining.** The immunostaining in the rodents is very different from the primates, and the three rodents differed from each other.

**Rat.** NPNFP staining in rat is relatively uniform over the depth of the DCN, with no well-defined laminar organization (Fig. 8A). There are stained puncta and fragments of processes; some large somata are outlined (example at Fig. 8B, arrow). With nNOS, there is dark staining of the outermost 50–100  $\mu\text{m}$  of the DCN (Fig. 8C, arrowhead), and then even staining of the full depth of the DCN to the level of the border with the icp. A higher magnification image shows stained somata and proximal processes of neurons (Fig. 8D, arrowhead) as well as scattered darkly stained puncta (Fig. 8D, arrow). Figure 8E, F shows that with GAD-immunoreactivity there is a band of dense staining of puncta that extends approximately half of the depth of the DCN (Fig. 8E, arrowhead marks the border of the darker region. Figure 8F shows the punctate GAD-immunostaining at higher magnification).

Figure 8G shows a band of darker CB-immunostaining in about the outer 100–200  $\mu\text{m}$  of the DCN (white arrowhead); this band contains many immunostained somata about 20  $\mu\text{m}$  in diameter (Fig. 8H, example at arrow). With CR immunostaining there is an outer layer with

few stained profiles (Fig. 8I) and a deeper broad band with many CR-ir neurons most with round somata (Fig. 8J, example at arrow). Finally, Fig. 8K, L show that there were PV-ir somata (Fig. 8L, arrow) scattered through about the outer layers of the DCN.

**Guinea pig.** NPNFP immunostaining in the guinea pig marked an outer band (Fig. 9A, arrowhead) of darker staining. Figure 9B shows that this band consists of stained somata (example at arrow) and processes, many of which are oriented perpendicular to the surface. However, nNOS staining is very light (Fig. 9C) with only a few scattered stained profiles (Fig. 9D) and no well-defined laminar organization. There also are nNOS-ir cells deep to the DCN (Fig. 9C, arrow). GAD immunoreactivity is seen in scattered small elements in about the outer half of the DCN (Fig. 9E,F). CB-immunoreactivity defined a darker outer region (Fig. 9G, arrowhead). There are CB-ir somata, (Fig. 9H, arrow) and processes in this darker band. CR immunoreactivity is observed in labeled scattered small cells (Fig. 9I, example at arrow); Eps8, a UBC marker (Sekerova et al., 2007; Manohar et al., 2012) also labels scattered somata (Fig. 9J, example at arrow). Finally, PV-ir in this species (Fig. 9K, L) shows a row of fusiform-shaped cells, a pattern not seen in any other animal.

**Chinchilla.** The pattern of NPNFP immunostaining (Fig. 10A,B) is similar to the pattern in the guinea pig. NPNFP-ir is present in vertically oriented processes (Fig. 10B, arrow) and puncta in layer 1. The pattern with nNOS is also similar to that seen in the rat, with staining darker over the outer half of the DCN (Fig. 10C, arrowhead) and scattered stained somata (Fig. 10D, example at arrow). Calcium-binding proteins instead mark different populations of neurons. CB-immunoreactivity stains the outer 100–200  $\mu\text{m}$  of the DCN (Fig. 10E, arrowhead). The staining is interrupted by unstained circular areas that may correspond to the patches of granule cells seen in the CV sections. Figure 10F shows that there are many stained round somata and processes (example at arrow). There are scattered CR-ir somata in layer 1 (Fig. 10G, arrow) and a broad band of stained elements in layer 2 (Fig. 10G, arrowhead). The inset shows that in this species Eps8 stains a scattering of somata. PV-ir marks round or oval (but not fusiform) somata (arrow, Fig. 10H).

## DISCUSSION

Our results suggest that the human DCN has a laminar organization and multiple neuron types as in other species. The neurochemical organization in the human DCN is similar, but not identical to that in macaque monkey, and both were different from the cat and the rodents, which in turn differed from each other. We will first review the patterns of laminar organization and then compare the neurochemically characterized neurons with the DCN neuron types that have been previously described.

### Laminar Organization

Laminar organization in the human is suggested by CV staining and by all of the markers we used. CV

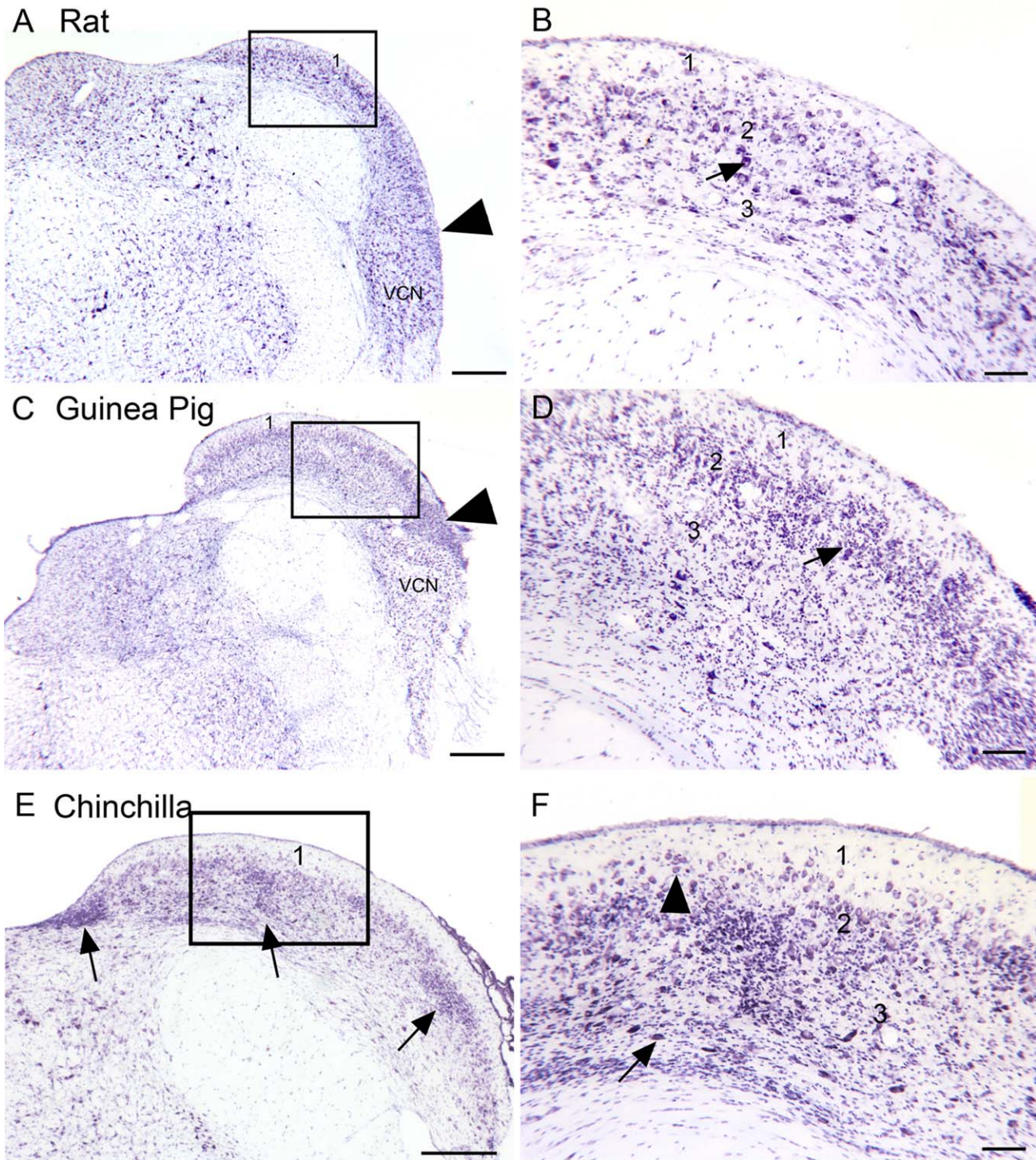


Fig. 7. Cytoarchitectural organization in the rat (**A, B**), guinea pig (**C, D**) and chinchilla (**E, F**). **A:** Low magnification image of the brainstem of the rat at a level where the DCN and VCN are both present. The arrowhead indicates the GCD. The outer lightly stained layer is marked with a "1." The rectangle shows the area in B. **B:** Higher magnification image of the rat DCN showing scattered neurons with large somata in layer 2 (example at arrow). **C:** Guinea pig the outer layer (1) again has relatively few stained somata and a large region of granule cells (arrowhead) is inserted between the DCN and the VCN. The rectangle

shows the location of the image in D. **D:** Layer 2 is distinguished by dense granule cells and scattered larger somata (example at arrow). **E:** Low magnification image of a CV-stained section through the DCN of a chinchilla. The arrows indicate several pools of darkly stained small neurons. **F:** Higher magnification image shows CV-stained somata of a variety of shapes, sizes, and orientations. The arrowhead shows a small neuron, the arrow shows a neuron with an elongated soma located deep in the cell layers of the DCN. Scale bars: A, C, E= 500  $\mu$ m; B, D, F= 100  $\mu$ m.

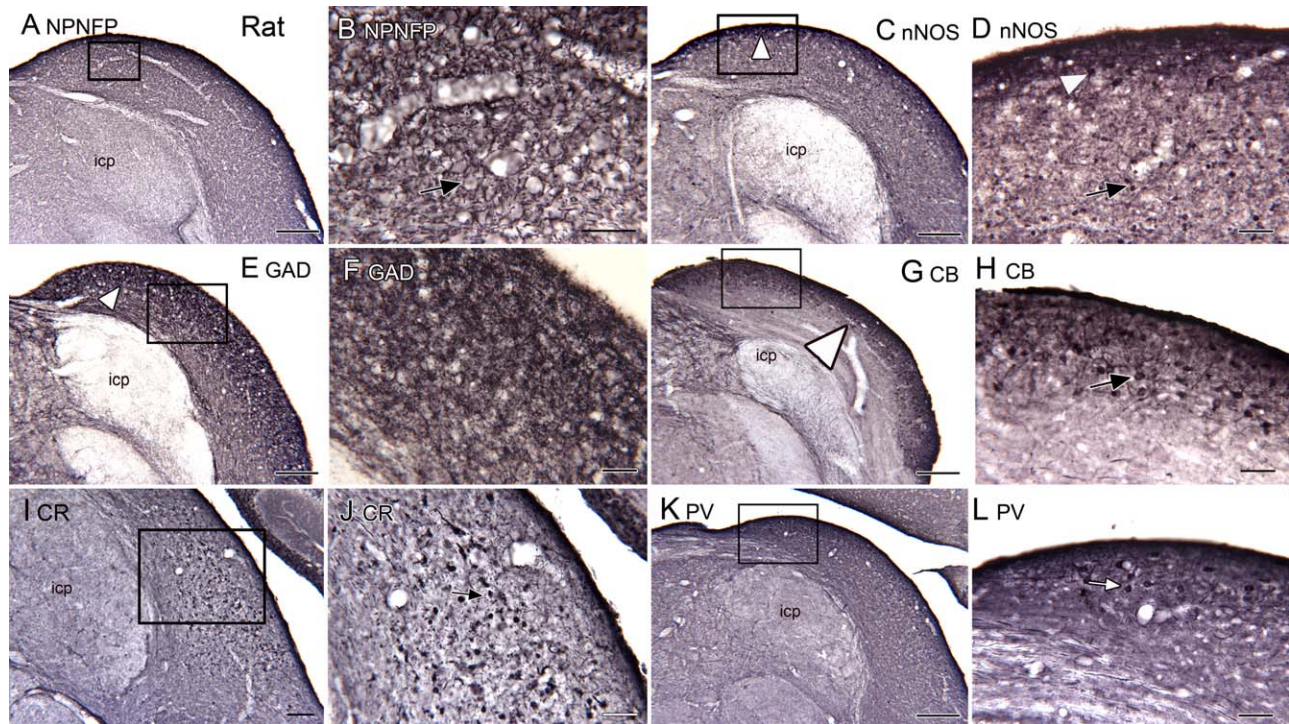


Fig. 8. The DCN in the rat. The images are arranged in pairs with a low magnification image on the left (A, C, E, G, I, K). The rectangles show the location of the higher magnification images to the right (B, D, F, H, J, L). **A:** NPNFP immunostaining is relatively uniform through the depth of the DCN. **B:** The higher magnification image shows that NPNFP is expressed in puncta and scattered fragments of processes; some staining surrounds large somata (example at arrow). **C:** With nNOS, there is a band of darker staining along approximately the outer 50  $\mu\text{m}$  of the DCN. There are scattered stained somata in that band (arrowhead). **D:** There are scattered larger somata in the outer band (arrowhead) as well as deeper in the DCN (arrow). **E:** GAD stain-

ing is punctate and denser in the outer half of the DCN. **F:** The punctate nature of GAD staining with occasional stained somata is clear at this magnification. **G:** Relatively uniform CB immunostaining with scattered somata in the outer layers. **H:** This higher magnification image shows scattered stained somata (example at arrow) in the outer layers of the DCN. **I:** CR immunostaining in the DCN; the outermost layer has fewer stained elements. **J:** Higher magnification image showing small, round, stained somata (example at arrow). **K:** PV immunoreactivity in the DCN. **L:** Higher magnification image showing stained somata (arrow) in the outer layer. Scale bars: A, C, E, G, K = 250  $\mu\text{m}$ ; B, D, F, H, J, L = 50  $\mu\text{m}$ ; I = 100  $\mu\text{m}$ .

staining suggests two layers, an outer lightly stained band ("1") and a broader band with many stained somata ("2"). This laminar organization is much more dramatically visualized with immunoreactivity for NPNFP. Beneath an outer, unstained layer is a very darkly stained band about 700  $\mu\text{m}$  deep with a population of well-stained neurons with fusiform or pyramidal somata distributed throughout its depth. This band is likely to correspond to the combined layers 2 and 3 as defined in other species, as suggested by Moore and Osen (1979). A laminar organization is also shown by immunoreactivity to the calcium-binding proteins. CB, CR, and PV stained fine fibers in the outer band. With PV, fibers deep to the DCN, presumably afferents, are also stained. The deepest band (3, seen with NPNFP, nNOS, and CR) corresponds to the fibers of the das.

### Monkey, Cat, Rodents

For all other species, CV staining showed an outer, molecular layer with few stained somata and below that a broad band of stained somata. The differentiation of this broad band into a distinct layer 2, a fusiform or pyramidal cell layer, and a layer 3, with a variety of neuron types, varies among species. In our sections, a

row of somata defining layer 2 is clearest in the cat, and visible in monkey and guinea pig sections. It is not as striking in rat and chinchilla; in those species the large neurons are scattered throughout a broader region (layers 2/3).

For the monkey, immunoreactivity for NPNFP is similar to human with a superficial lightly stained band and a broad band of dark staining beneath it. NPNFP staining in the other species is very different, with a band of darker staining in the superficial DCN that does not overlap the larger projection neurons as seen with CV staining. The laminar pattern for nNOS in cat and rodents is different from the pattern in human and monkey in that nNOS staining is darker in the more superficial DCN rather than in the region defined by NPNFP immunostaining.

These observations basically confirm many earlier studies on the laminar organization of the DCN in the cat (Brawer et al., 1974; Blackstad et al., 1984), monkey (Rubio et al., 2008), chinchilla (Fleckenstein et al., 1991), guinea pig (Hackney et al., 1990) and rat (Mugnaini et al., 1980a; Wouterlood et al., 1984; Mugnaini, 1985; Diño and Mugnaini, 2008). Our data in monkeys are in agreement with Rubio et al. (2008) in showing the existence of a molecular layer.

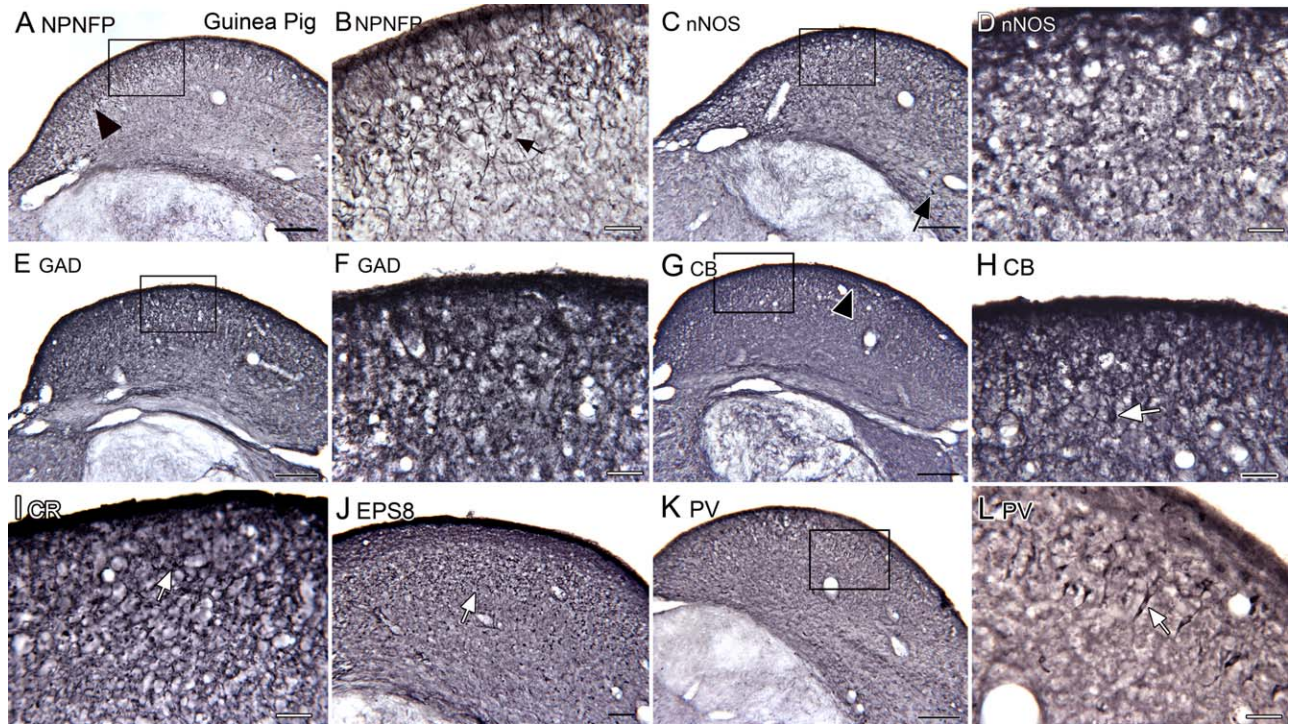


Fig. 9. The DCN in the guinea pig. **A:** NPNFP immunostaining marks a more darkly stained outer layer (arrowhead). The rectangle shows the region in **B**. The staining is composed of small stained somata (arrow) and processes, many of which are oriented perpendicular to the surface. **C:** nNOS immunostaining is relatively light and uniform. A few stained somata are seen deep in the DCN (arrow). The rectangle shows the region in **D**. The higher magnification image shows scattered puncta of a variety of sizes. **E:** GAD immunostaining is punctate and again relatively uniform. **F:** The punctate nature of GAD immuno-

staining shown at higher magnification. **G:** CB staining marks an outer darker band (arrowhead). **H:** The band is comprised of stained small somata and processes. **I:** CR immunostaining marks stained processes and puncta. **J:** Eps8 staining shows many stained widely distributed somata. **K:** Parvalbumin immunostaining distinguishes the outer third of the DCN. The rectangle shows the region in **L**. **L:** Neurons with fusiform somata (example at arrow) oriented perpendicular to the surface are stained with PV. Scale bars: A, C, E, G, K = 250  $\mu$ m; B, D, F, H, I, L = 50  $\mu$ m; J = 100  $\mu$ m.

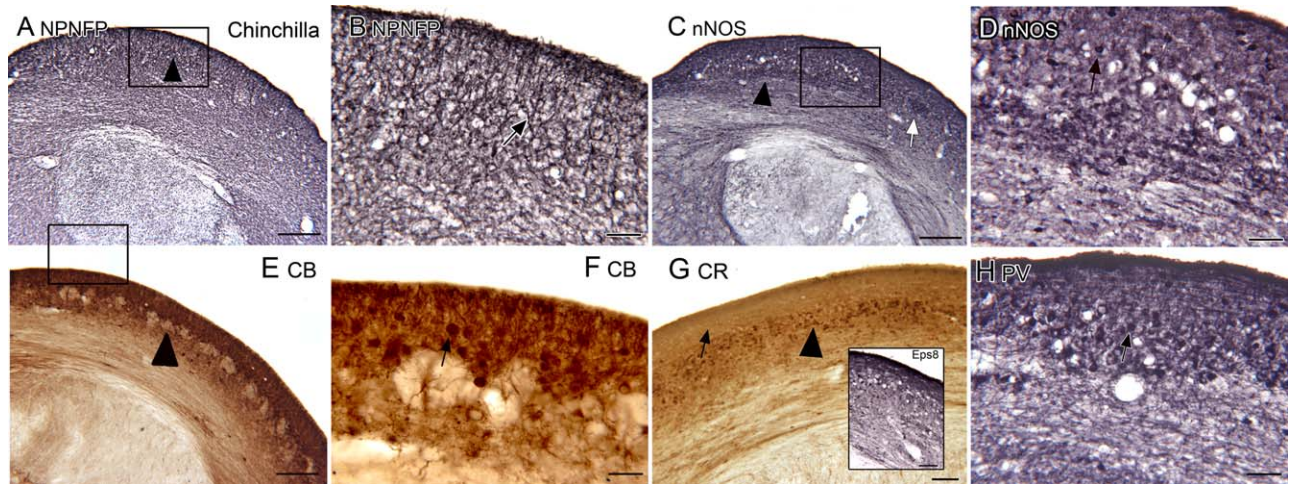


Fig. 10. The DCN in the chinchilla. **A:** NPNFP immunostaining is denser in the outer layers; arrowhead marks the border of the darker staining. **B:** There are stained processes (example at arrow) in the outer 200  $\mu$ m of the DCN, many oriented perpendicular to the surface. **C:** nNOS immunoreactivity is darker in the outer region (arrowhead at border). The rectangle shows the location of the image in **D**. **D:** There are scattered nNOS-ir somata (example at arrow). **E:** CB-ir. The outer layer (arrowhead) is more darkly stained. Note the circular regions of

lighter staining. The rectangle shows the location of the image in **F**. **F:** There are many stained somata (example at arrow) and processes in the outer layer. **G:** CR. The outer layer is lightly stained; beneath it are stained somata and processes. The inset shows that immunoreactivity for Eps8 overlaps but is not coextensive with the CR immunoreactivity. **H:** PV-ir somata in the superficial DCN. Scale bars: A, C, E = 250  $\mu$ m; B, D, F, H = 50  $\mu$ m; G and inset = 100  $\mu$ m.

## Granule Cell Domain

Another characteristic of the cochlear nuclear complex in nonhuman species is the presence of a region of dense granule cells between the DCN and VCN, the GCD. While the staining pattern in the DCN is distinct from the more ventral VCN (for example Fig. 1C), we did not see a GCD in any of the CV-stained sections from the human cases. We did not examine serial sections through the entire DCN/VCN so the existence of a granule cell domain in human cannot be definitively ruled out from our data, but other studies have argued that a GCD is absent in humans (Wagoner and Kulesza, 2009). A GCD is apparent in CV staining for the other species, including the macaque monkey.

## Cell Types in the DCN

The cell types of the DCN have been characterized in other species by Golgi, Nissl, and immunohistochemical staining. The model of DCN circuitry (Oertel and Young, 2004) identifies these cell types and shows their synaptic relations to each other. How do the neurons we see labeled with different markers fit into this scheme?

## NPNFP

In the human, NPNFP is prominently expressed in a population of well-stained neurons with fusiform or pyramidal somata distributed throughout the depth of band 2. We propose that the NPNFP-ir neurons are the output neurons of the human DCN, the human equivalent of the pyramidal or fusiform cells. This suggestion is based in part on studies on other brain regions in which NPNFP has been found to be a marker for glutamatergic cells with long projections, e.g. pyramidal cells of the cerebral cortex of many species (Hof and Morrison, 1990; Hof et al., 1990, 1995, 1997; King et al., 2001; Boire et al., 2005; Van der Gucht et al., 2006; Van der Gucht et al., 2007; Paulussen et al., 2011) and somata of cranial nerve nuclei in the brainstem (Baizer, 2009; Baizer et al., 2011a). In the macaque monkey, NPNFP also defined a broad band of staining made up of stained neurons and processes; the stained neurons may represent the projection neurons.

NPNFP, however, is not expressed in the projection neurons in any of the other species. There are stained elements, but these are more superficially located than the projection neurons. This variability in NPNFP expression is in contrast to the cerebral cortex; NPNFP is expressed in pyramidal cells in all mammalian species examined to date (Campbell et al., 1991; Hof et al., 1992, 1995, 1996, 1997; Boire et al., 2005; Van der Gucht et al., 2007; Sherwood et al., 2009; Paulussen et al., 2011; Ouda et al., 2012). NPNFP expression in the DCN reveals a major difference in neurochemistry between primates and nonprimates.

## nNOS

In human there are scattered somata in the broad band defined by NPNFP staining. Some somata are elongated parallel to the DCN border; a few immunolabeled neurons and processes are seen in the underlying das. In the macaque monkey, there is also staining of elongated somata overlapping the NPNFP band. These profiles have shapes

similar to the nNOS-ir neurons in human. Although spatially overlapped, the nNOS and NPNFP-ir neurons probably represent different populations, as double-labeling in macaque monkey showing that the NPNFP and nNOS are expressed in different cells. nNOS-ir somata are quite different in the other species, both in laminar location and in appearance. In the cat, nNOS immunostaining labels neurons in the molecular layer. In all three rodents, rat, chinchilla and guinea pig, there are nNOS-ir neurons in the molecular layer and in deeper layers. Studies in different parts of the CNS have shown that nNOS is typically expressed in GABAergic interneurons and not glutamatergic projection neurons (Valtschanoff et al., 1993, 1995; Smiley et al., 2000; Jinno and Kosaka, 2002; Fuentealba et al., 2008). Inhibitory interneurons in the cat and rodent DCN include stellate, cartwheel and Golgi cells (Oertel and Young, 2004); in cat and rodent the nNOS-ir population may represent one or more of those classes. In the primates nNOS immunoreactivity may also mark inhibitory interneurons but the labeled cells have a very different morphology from the cells labeled in cat and rodent.

## Calcium-Binding Proteins

**CB.** Immunoreactivity for CB has been described in three cell populations: cartwheel cells of the molecular layer (Zettel et al., 1991, bat; Frisina et al., 1995, chinchilla; Spatz, 1997, guinea pig, strongly; rat, weakly; Rubio et al., 2008, macaque monkey), Purkinje-like cells (Spatz, 1997, 2003, tree shrew, rat and guinea pig) and UBCs (but only in the marmoset and not in rat or guinea pig (Spatz, 2000). Cartwheel cells are also labeled with two other antibodies, one against PEP-19, a calcium-binding protein (Berrebi and Mugnaini, 1991, guinea pig) and the other against the IP3 receptor (Ryugo et al., 1995, many species including humans).

We did not see profiles resembling cartwheel cells in the human CB-ir sections. We did see CB-ir Purkinje-like cells in the human, suggesting both that there is CB expression and that our methods are sufficient to detect it. In the macaque monkey, only a few scattered profiles are CB-ir; again cells resembling cartwheel cells are not labeled.

In contrast, many CB-ir neurons, variously in layers 1 and 2/3 are found in all other species. Some or all of these neurons probably correspond to cartwheel cells.

**CR.** In earlier studies in the rat, CR expression has been shown in UBCs and in scattered somata in layers 2 and 3 of the DCN (Arai et al., 1991, Fig. 13B; Floris et al., 1994; Spatz, 2000; Manohar et al., 2012). In the human, CR labeled processes running along the length of the DCN in the outermost layer. In band 2, both processes and small somata are labeled. In the macaque monkey, CR-ir neurons are found within the region marked by NPNFP-immunoreactivity. The CR immunolabeling pattern varied among the other species. In the cat, very few somata are labeled whereas in rat and guinea pig there are many scattered somata. In the chinchilla, CR is present in a broad band of cells below the molecular layer. CR labels a subset of UBCs (Floris et al., 1994; Mugnaini et al., 2011); some of the stained elements are probably UBCs. We also compared staining with CR and Eps8, a pan-UBC marker (Sekerikova et al., 2007) in guinea pig and chinchilla. We found different patterns of

labeling for these markers, suggesting that there may be additional populations of UBCs that are not CR-ir (as in the mouse, Nunzi et al., 2002; Chung et al., 2009).

**PV.** The earlier results with PV-ir are inconsistent among species. Celio (1990) did not find PV-ir somata in rat DCN although he did describe PV-ir beaded axons and terminals. By contrast, Bazwinsky et al. (2008) reported PV-immunoreactivity in all DCN neurons. We found major differences among species in staining for PV. In humans, PV also stained long beaded fibers in both the molecular layer and in band 2. In the cat the PV did not stain processes but somata scattered in the entire width of the DCN. In the guinea pig, somata of fusiform cells are PV-ir. In the chinchilla and the rat, there are PV-ir somata in the molecular layer. Again, these may represent a population of inhibitory interneurons.

**GAD.** The staining with the GAD antibody we used, yielded similar results in all species with dense punctate label throughout the DCN. We had hoped to label GABAergic cells in the DCN but the dense label made it very difficult to see labeled somata. The punctate label suggests heavy inhibitory input to the DCN. This might include both local circuit inhibitory neurons, as well as descending GABAergic axons from the trapezoid body or superior olivary complex (Ostapoff et al., 1997).

### Species Variability in DCN Neurochemistry

The expression of NPNFP and nNOS distinguishes primates from nonprimates. We also found differences in the expression of calcium-binding proteins between humans and other species, as well as more subtle differences among the species. In the human, none of the calcium-binding proteins labeled large somata. In the other species, calcium-binding proteins labeled populations of neurons although the shapes and distribution of neurons identified by the different proteins vary among species. The species variability in expression of calcium-binding proteins in defined cell classes have been reported previously for the DCN as well as for other structures (Spatz, 1997; Hof et al., 1999; Spatz, 2000; Seress et al., 2008; Morona and Gonzalez, 2009). Different physiological characteristics are associated with the expression of different calcium-binding proteins (Baimbridge et al., 1992; Schwaller et al., 2002; Schwaller, 2010); there may therefore be species differences, perhaps subtle ones, in the physiological properties of neurons assigned to the same class reflecting different calcium-binding protein expression.

### Cell Types and Circuitry in the Human DCN

We have identified two neurochemical cell types, the NPNFP-ir and nNOS-ir neuronal populations in human and macaque monkey that do not have neurochemical counterparts in the other species. In human, there are rare examples of other cell types, namely, a large nNOS-ir cell in the molecular layer, and a few CB-ir Purkinje-like cells.

The granule cell is a critical component of DCN circuitry (Mugnaini et al., 1980a; Mugnaini et al., 1980b; Oertel and Young, 2004). We suggest that there may be a granule cell population in the human that is CR- or CB-ir or both. In other species, the axons of these cells

form parallel fibers that run along the molecular layer and innervate dendrites of cartwheel and fusiform cells (summary in Oertel and Young, 2004); our data argue against this arrangement in the human. In the human sections there is a clearly demarcated molecular layer with fine beaded fibers that may represent the axons of granule cells; we did not, however, label dendrites of either putative projection neurons or interneurons extending into that layer.

Other key components of DCN circuitry are inhibitory interneurons (cartwheel cells, stellate cells, Golgi cells, tuberculoventral cells). While candidate inhibitory interneurons are stained by nNOS and/or calcium-binding proteins in the monkey, cat, and rodents, there are no such neurons stained in the human. Those markers are effective in labeling other elements in the human tissue, suggesting that if these inhibitory interneurons exist in humans they have very different neurochemical properties. Earlier studies in the human using other markers have identified UBCs (Spatz, 2001) and a putative cartwheel cell population (Ryugo et al., 1995) in the human DCN.

These data imply a different circuit diagram for the human DCN than that established for other mammals (Oertel and Young, 2004, Fig. 1). The suggestion that the organization and cell types in the human DCN are different than in non-primates is consistent with early descriptions (Moore and Osen, 1979; Moore, 1980; Heiman-Patterson and Strominger, 1985; Adams, 1986).

Finally, we should consider the possible functional implications of these species differences in DCN organization. Tinnitus, the perception of a phantom sound, is a major human health problem. The locus and mechanisms leading to tinnitus, while intensively studied, are not understood (discussion and references in Kaltenbach, 2006a; Roberts et al., 2010; Kaltenbach, 2011; Wang et al., 2011; Baizer et al., 2012a). Data from animal studies implicate the DCN in tinnitus (Brozoski et al., 2002; Kaltenbach, 2006a,b; Dehmel et al., 2012). Do these results generalize to humans? Our data suggest that there may be major differences in the circuitry of the human DCN compared with rodents so that the changes in the physiology of the DCN described in rodents may not be applicable to humans.

### ACKNOWLEDGMENTS

The authors thank Debra Kigar in Dr. Witelson's laboratory for the dissection of the brainstems. They thank Dr. Susan Shore for the gift of two guinea pig brains and for her comments on an earlier draft of this manuscript. Dr. David Bender, University at Buffalo, donated the brains of monkeys A and B. They thank Dr. Paul J. May for his very careful critique of an earlier version of the manuscript. They thank the Confocal Microscope and Flow Cytometry Faculty in the School of Medicine and Biomedical Sciences for use of the Zeiss Axioimager microscope.

### LITERATURE CITED

- Adams JC. 1986. Neuronal morphology in the human cochlear nucleus. *Arch Otolaryngol Head Neck Surg* 112:1253-1261.
- Adams JC, Warr WB. 1976. Origins of axons in the cat's acoustic striae determined by injection of horseradish peroxidase into severed tracts. *J Comp Neurol* 170:107-121.

- André VM, Cepeda C, Vinters HV, Huynh M, Mathern GW, Levine MS. 2008. Pyramidal cell responses to gamma-aminobutyric acid differ in type I and type II cortical dysplasia. *J Neurosci Res* 86:3151–3162.
- Arai R, Winsky L, Arai M, Jacobowitz DM. 1991. Immunohistochemical localization of calretinin in the rat hindbrain. *J Comp Neurol* 310:21–44.
- Armstrong C, Szabadies J, Tamas G, Soltesz I. 2011. Neurogliaform cells in the molecular layer of the dentate gyrus as feed-forward gamma-aminobutyric acidergic modulators of entorhinal-hippocampal interplay. *J Comp Neurol* 519:1476–1491.
- Baimbridge KG, Celio MR, Rogers JH. 1992. Calcium-binding proteins in the nervous system. *Trends Neurosci* 15:303–308.
- Baizer JS. 2009. Nonphosphorylated neurofilament protein is expressed by scattered neurons in the vestibular and precerebellar brainstem. *Brain Res* 1298:46–56.
- Baizer JS, Baker JF. 2005. Immunoreactivity for calcium-binding proteins defines subregions of the vestibular nuclear complex of the cat. *Exp Brain Res* 164:78–91.
- Baizer JS, Baker JF. 2006a. Immunoreactivity for calretinin and calbindin in the vestibular nuclear complex of the monkey. *Exp Brain Res* 172:103–113.
- Baizer JS, Baker JF. 2006b. Neurochemically defined cell columns in the nucleus prepositus hypoglossi of the cat and monkey. *Brain Res* 1094:127–137.
- Baizer JS, Baker JF, Haas K, Lima R. 2007. Neurochemical organization of the nucleus paramedianus dorsalis in the human. *Brain Res* 1176:45–52.
- Baizer JS, Broussard DM. 2010. Expression of calcium-binding proteins and nNOS in the human vestibular and precerebellar brainstem. *J Comp Neurol* 518:872–895.
- Baizer JS, Corwin WL, Baker JF. 2010. Otolith stimulation induces c-Fos expression in vestibular and precerebellar nuclei in cats and squirrel monkeys. *Brain Res* 1351:64–73.
- Baizer JS, Manohar S, Paolone NA, Weinstock N, Salvi RJ. 2012a. Understanding tinnitus: the dorsal cochlear nucleus, organization and plasticity. *Brain Res* 1485:40–53.
- Baizer JS, Paolone N, Weinstock N. 2013a. Laminar and cellular organization of the human dorsal cochlear nucleus. ARO program, #649.
- Baizer JS, Paolone NA, Witelson SF. 2011a. Nonphosphorylated neurofilament protein is expressed by scattered neurons in the human vestibular brainstem. *Brain Res* 1382:45–56.
- Baizer JS, Paolone NA, Witelson SF. 2011b. Nonphosphorylated neurofilament protein is expressed by scattered neurons in the human vestibular brainstem. *Brain Res* 1382:45–56.
- Baizer JS, Sherwood CC, Hof PR, Witelson SF, Sultan F. 2011c. Neurochemical and structural organization of the principal nucleus of the inferior olive in the human. *Anat Rec* 294:1198–1216.
- Baizer JS, Weinstock N, Paolone N, Ng J, Witelson SF. 2012b. Structure of the human dorsal cochlear nucleus. *Neuroscience Meeting Planner New Orleans, LA Society for Neuroscience, 2012 Online Program No. 363.09.*
- Baizer JS, Weinstock N, Witelson SF, Sherwood CC, Hof PR. 2013b. The nucleus parabrachialis in the human, chimpanzee, and macaque monkey. *Brain Struct Funct* 218:389–403.
- Barnes W, Magoun H, Ranson S. 1943. The ascending auditory pathway in the brain stem of the monkey. *J Comp Neurol* 79:129–152.
- Bazwinsky I, Hartig W, Rubsam R. 2008. Characterization of cochlear nucleus principal cells of *Meriones unguiculatus* and *Monodelphis domestica* by use of calcium-binding protein immunolabeling. *J Chem Neuroanat* 35:158–174.
- Belenky MA, Yarom Y, Pickard GE. 2008. Heterogeneous expression of gamma-aminobutyric acid and gamma-aminobutyric acid-associated receptors and transporters in the rat suprachiasmatic nucleus. *J Comp Neurol* 506:708–732.
- Berman A. 1968. The brain stem of the cat. Madison, WI: University of Wisconsin Press.
- Berberi AS, Mugnaini E. 1991. Distribution and targets of the cartwheel cell axon in the dorsal cochlear nucleus of the guinea pig. *Anat Embryol* 183:427–454.
- Blackstad TW, Osen KK, Mugnaini E. 1984. Pyramidal neurones of the dorsal cochlear nucleus: a Golgi and computer reconstruction study in cat. *Neuroscience* 13:827–854.
- Boire D, Desgent S, Matteau I, Ptito M. 2005. Regional analysis of neurofilament protein immunoreactivity in the hamster's cortex. *J Chem Neuroanat* 29:193–208.
- Brawer JR, Morest DK, Kane EC. 1974. The neuronal architecture of the cochlear nucleus of the cat. *J Comp Neurol* 155:251–300.
- Brozoski TJ, Bauer CA, Caspary DM. 2002. Elevated fusiform cell activity in the dorsal cochlear nucleus of chinchillas with psychophysical evidence of tinnitus. *J Neurosci* 22:2383–2390.
- Campbell MJ, Hof PR, Morrison JH. 1991. A subpopulation of primate corticocortical neurons is distinguished by somatodendritic distribution of neurofilament protein. *Brain Res* 539:133–136.
- Cant NB, Benson CG. 2003. Parallel auditory pathways: projection patterns of the different neuronal populations in the dorsal and ventral cochlear nuclei. *Brain Res Bull* 60:457–474.
- Celio MR. 1990. Calbindin D-28k and parvalbumin in the rat nervous system. *Neuroscience* 35:375–475.
- Chung S-H, Marzban H, Watanabe M, Hawkes R. 2009. Phospholipase Cbeta4 expression identifies a novel subset of unipolar brush cells in the adult mouse cerebellum. *Cerebellum* 8:267–276.
- Dehmel S, Pradhan S, Koehler S, Bledsoe S, Shore S. 2012. Noise overexposure alters long-term somatosensory-auditory processing in the dorsal cochlear nucleus—possible basis for tinnitus-related hyperactivity? *J Neurosci* 32:1660–1671.
- Delaunay D, Heydon K, Miguez A, Schwab M, Nave KA, Thomas JL, Spassky N, Martinez S, Zalc B. 2009. Genetic tracing of subpopulation neurons in the prethalamus of mice (*Mus musculus*). *J Comp Neurol* 512:74–83.
- Diño MR, Mugnaini E. 2008. Distribution and phenotypes of unipolar brush cells in relation to the granule cell system of the rat cochlear nucleus. *Neuroscience* 154:29–50.
- Disterhoft JF, Perkins RE, Evans S. 1980. Neuronal morphology of the rabbit cochlear nucleus. *J Comp Neurol* 192:687–702.
- Felch DL, Van Hooser SD. 2012. Molecular compartmentalization of lateral geniculate nucleus in the gray squirrel (*Sciurus carolinensis*). *Front Neuroanat* 6:12.
- Fleckeisen CE, Harrison RV, Mount RJ. 1991. Cytoarchitecture of cochlear nucleus in the chinchilla. *Acta Otolaryngol Suppl* 489:12–22.
- Floris A, Diño M, Jacobowitz DM, Mugnaini E. 1994. The unipolar brush cells of the rat cerebellar cortex and cochlear nucleus are calretinin-positive: a study by light and electron microscopic immunocytochemistry. *Anat Embryol* 189:495–520.
- Frisina RD, Zettl ML, Kelley PE, Walton JP. 1995. Distribution of calbindin D-28k immunoreactivity in the cochlear nucleus of the young adult chinchilla. *Hear Res* 85:53–68.
- Fuentealba P, Begum R, Capogna M, Jinno S, Marton LF, Csicsvari J, Thomson A, Somogyi P, Klausberger T. 2008. Ivy cells: a population of nitric-oxide-producing, slow-spiking GABAergic neurons and their involvement in hippocampal network activity. *Neuron* 57:917–929.
- Gacek RR. 1973. A cerebellocochlear nucleus pathway in the cat. *Exp Neurol* 41:101–112.
- Hackney CM, Osen KK, Kolston J. 1990. Anatomy of the cochlear nuclear complex of guinea pig. *Anat Embryol* 182:123–149.
- Heiman-Patterson TD, Strominger NL. 1985. Morphological changes in the cochlear nuclear complex in primate phylogeny and development. *J Morphol* 186:289–306.
- Hof PR, Cox K, Morrison JH. 1990. Quantitative analysis of a vulnerable subset of pyramidal neurons in Alzheimer's disease. I. Superior frontal and inferior temporal cortex. *J Comp Neurol* 301:44–54.
- Hof PR, Glezer II, Archin N, Janssen WG, Morgane PJ, Morrison JH. 1992. The primary auditory cortex in cetacean and human brain: a comparative analysis of neurofilament protein-containing pyramidal neurons. *Neurosci Lett* 146:91–95.

- Hof PR, Glezer II, Condé F, Flagg RA, Rubin MB, Nimchinsky EA, Vogt Weisenhorn DM. 1999. Cellular distribution of the calcium-binding proteins parvalbumin, calbindin, and calretinin in the neocortex of mammals: phylogenetic and developmental patterns. *J Chem Neuroanat* 16:77–116.
- Hof PR, Morrison JH. 1990. Quantitative analysis of a vulnerable subset of pyramidal neurons in Alzheimer's disease. II. Primary and secondary visual cortex. *J Comp Neurol* 301:55–64.
- Hof PR, Nimchinsky EA, Morrison JH. 1995. Neurochemical phenotype of corticocortical connections in the macaque monkey: quantitative analysis of a subset of neurofilament protein-immunoreactive projection neurons in frontal, parietal, temporal, and cingulate cortices. *J Comp Neurol* 362:109–133.
- Hof PR, Ungerleider LG, Adams MM, Webster MJ, Gattass R, Blumberg DM, Morrison JH. 1997. Callosally projecting neurons in the macaque monkey V1/V2 border are enriched in nonphosphorylated neurofilament protein. *Vis Neurosci* 14:981–987.
- Hof PR, Ungerleider LG, Webster MJ, Gattass R, Adams MM, Sailstad CA, Morrison JH. 1996. Neurofilament protein is differentially distributed in subpopulations of corticocortical projection neurons in the macaque monkey visual pathways. *J Comp Neurol* 376:112–127.
- Jinno S, Kosaka T. 2002. Patterns of expression of calcium binding proteins and neuronal nitric oxide synthase in different populations of hippocampal GABAergic neurons in mice. *J Comp Neurol* 449:1–25.
- Kaltenbach JA. 2006a. The dorsal cochlear nucleus as a participant in the auditory, attentional and emotional components of tinnitus. *Hear Res* 216-217:224–234.
- Kaltenbach JA. 2006b. Summary of evidence pointing to a role of the dorsal cochlear nucleus in the etiology of tinnitus. *Acta Otolaryngol (Suppl)*:20–26.
- Kaltenbach JA. 2011. Tinnitus: Models and mechanisms. *Hear Res* 276:52–60.
- King CE, Canty AJ, Vickers JC. 2001. Alterations in neurofilaments associated with reactive brain changes and axonal sprouting following acute physical injury to the rat neocortex. *Neuropathol Appl Neurobiol* 27:115–126.
- Ksiezak-Reding H, Dickson DW, Davies P, Yen SH. 1987. Recognition of tau epitopes by anti-neurofilament antibodies that bind to Alzheimer neurofibrillary tangles. *Proc Natl Acad Sci USA* 84:3410–3414.
- LaBossiere E, Glickstein M. 1976. *Histological processing for the neural sciences*. Springfield, IL: Charles C. Thomas.
- Lee VM, Otvos L, Jr., Carden MJ, Hollosi M, Dietzschold B, Lazzarini RA. 1988. Identification of the major multiphosphorylation site in mammalian neurofilaments. *Proc Natl Acad Sci USA* 85:1998–2002.
- Liguz-Leczna M, Waleszczyk WJ, Zakrzewska R, Skangiel-Kramska J, Kossut M. 2009. Associative pairing involving monocular stimulation selectively mobilizes a subclass of GABAergic interneurons in the mouse visual cortex. *J Comp Neurol* 516:482–492.
- Liodis P, Denaxa M, Grigoriou M, Akufo-Addo C, Yanagawa Y, Pachnis V. 2007. Lhx6 activity is required for the normal migration and specification of cortical interneuron subtypes. *J Neurosci* 27:3078–3089.
- Lorente de Nó R. 1933. Anatomy of the eighth nerve. III. General plan of structure of the primary cochlear nuclei. *Laryngoscope* 43:327–350.
- Lorente de Nó R. 1981. *The primary acoustic nuclei*. New York: Raven Press.
- Manohar S, Paolone NA, Bleichfeld M, Hayes SH, Salvi RJ, Baizer JS. 2012. Expression of doublecortin, a neuronal migration protein, in unipolar brush cells of the vestibulocerebellum and dorsal cochlear nucleus of the adult rat. *Neuroscience* 202:169–183.
- Masterton RB, Granger EM. 1988. Role of the acoustic striae in hearing: contribution of dorsal and intermediate striae to detection of noises and tones. *J Neurophysiol* 60:1841–1860.
- Moore JK. 1980. The primate cochlear nuclei: loss of lamination as a phylogenetic process. *J Comp Neurol* 193:609–629.
- Moore JK, Osen KK. 1979. The cochlear nuclei in man. *Am J Anat* 154:393–418.
- Moore JK, Osen KK, Storm-Mathisen J, Ottersen OP. 1996. gamma-Aminobutyric acid and glycine in the baboon cochlear nuclei: an immunocytochemical colocalization study with reference to interspecies differences in inhibitory systems. *J Comp Neurol* 369:497–519.
- Morona R, Gonzalez A. 2009. Immunohistochemical localization of calbindin-D28k and calretinin in the brainstem of anuran and urodele amphibians. *J Comp Neurol* 515:503–537.
- Mugnaini E. 1985. GABA neurons in the superficial layers of the rat dorsal cochlear nucleus: light and electron microscopic immunocytochemistry. *J Comp Neurol* 235:61–81.
- Mugnaini E, Osen KK, Dahl AL, Friedrich VL, Jr., Korte G. 1980a. Fine structure of granule cells and related interneurons (termed Golgi cells) in the cochlear nuclear complex of cat, rat and mouse. *J Neurocytol* 9:537–570.
- Mugnaini E, Sekerkova G, Martina M. 2011. The unipolar brush cell: a remarkable neuron finally receiving deserved attention. *Brain Res Rev* 66:220–245.
- Mugnaini E, Warr WB, Osen KK. 1980b. Distribution and light microscopic features of granule cells in the cochlear nuclei of cat, rat, and mouse. *J Comp Neurol* 191:581–606.
- Nunzi MG, Shigemoto R, Mugnaini E. 2002. Differential expression of calretinin and metabotropic glutamate receptor mGluR1alpha defines subsets of unipolar brush cells in mouse cerebellum. *J Comp Neurol* 451:189–199.
- Oertel D, Young ED. 2004. What's a cerebellar circuit doing in the auditory system? *Trends Neurosci* 27:104–110.
- Olszewski J, Baxter D. 1954. *Cytoarchitecture of the human brain stem*, second ed. Basel: Karger.
- Osen KK. 1969. Cytoarchitecture of the cochlear nuclei in the cat. *J Comp Neurol* 136:453–484.
- Ostapoff EM, Benson CG, Saint Marie RL. 1997. GABA- and glycine-immunoreactive projections from the superior olivary complex to the cochlear nucleus in guinea pig. *J Comp Neurol* 381:500–512.
- Ouda L, Druga R, Syka J. 2012. Distribution of SMI-32-immunoreactive neurons in the central auditory system of the rat. *Brain Struct Funct* 217:19–36.
- Paolone N, Manohar S, Hayes SH, Wong KM, Salvi RJ, Baizer JS. 2014. Dissociation of doublecortin expression and neurogenesis in unipolar brush cells in the vestibulocerebellum and dorsal cochlear nucleus of the adult rat. *Neuroscience* 265:323–331.
- Paulussen M, Jacobs S, Van der Gucht E, Hof PR, Arckens L. 2011. Cytoarchitecture of the mouse neocortex revealed by the low-molecular-weight neurofilament protein subunit. *Brain Struct Funct* 216:183–199.
- Paxinos G, Huang XF. 1995. *Atlas of the human brainstem*. San Diego: Academic Press.
- Rainnie DG, Mania I, Mascagni F, McDonald AJ. 2006. Physiological and morphological characterization of parvalbumin-containing interneurons of the rat basolateral amygdala. *J Comp Neurol* 498:142–161.
- Ramón y Cajal S. 1953. *Histologie du système nerveux de l'homme et des vertébrés*. Madrid: Consejo Superior de Investigaciones Científicas, Instituto Ramón y Cajal.
- Roberts LE, Eggermont JJ, Caspary DM, Shore SE, Melcher JR, Kaltenbach JA. 2010. Ringing ears: the neuroscience of tinnitus. *J Neurosci* 30:14972–14979.
- Rubio ME, Gudsnuk KA, Smith Y, Ryugo DK. 2008. Revealing the molecular layer of the primate dorsal cochlear nucleus. *Neuroscience* 154:99–113.
- Ryugo DK, Pongstaporn T, Wright DD, Sharp AH. 1995. Inositol 1,4,5-trisphosphate receptors: immunocytochemical localization in the dorsal cochlear nucleus. *J Comp Neurol* 358:102–118.
- Salgado H, Bellay T, Nichols JA, Bose M, Martinolich L, Perrotti L, Atzori M. 2007. Muscarinic M2 and M1 receptors reduce GABA release by Ca<sup>2+</sup> channel modulation through activation of PI3K/Ca<sup>2+</sup>-independent and PLC/Ca<sup>2+</sup>-dependent PKC. *J Neurophysiol* 98:952–965.
- Schmid RS, Tsujimoto N, Qu Q, Lei H, Li E, Chen T, Blaustein CS. 2008. A methyl-CpG-binding protein 2-enhanced green fluorescent

- protein reporter mouse model provides a new tool for studying the neuronal basis of Rett syndrome. *Neuroreport* 19:393–398.
- Schwaller B. 2010. Cytosolic  $Ca^{2+}$  buffers. *Cold Spring Harb Perspect Biol* 2:a004051.
- Schwaller B, Meyer M, Schiffmann S. 2002. 'New' functions for 'old' proteins: the role of the calcium-binding proteins calbindin D-28k, calretinin and parvalbumin, in cerebellar physiology. Studies with knockout mice. *Cerebellum* 1:241–258.
- Sekerkova G, Dino MR, Ilijic E, Russo M, Zheng L, Bartles JR, Mugnaini E. 2007. Postsynaptic enrichment of Eps8 at dendritic shaft synapses of unipolar brush cells in rat cerebellum. *Neuroscience* 145:116–129.
- Seress L, Abraham H, Czeh B, Fuchs E, Leranath C. 2008. Calretinin expression in hilar mossy cells of the hippocampal dentate gyrus of nonhuman primates and humans. *Hippocampus* 18:425–434.
- Sherwood CC, Stimpson CD, Butti C, Bonar CJ, Newton AL, Allman JM, Hof PR. 2009. Neocortical neuron types in Xenarthra and Afrotheria: implications for brain evolution in mammals. *Brain Struct Funct* 213:301–328.
- Smiley JF, McGinnis JP, Javitt DC. 2000. Nitric oxide synthase interneurons in the monkey cerebral cortex are subsets of the somatostatin, neuropeptide Y, and calbindin cells. *Brain Res* 863:205–212.
- Smith PH, Massie A, Joris PX. 2005. Acoustic stria: anatomy of physiologically characterized cells and their axonal projection patterns. *J Comp Neurol* 482:349–371.
- Spatz WB. 1997. Differences between guinea pig and rat in the dorsal cochlear nucleus: expression of calcium-binding proteins by cartwheel and Purkinje-like cells. *Hear Res* 107:136–146.
- Spatz WB. 2000. Unipolar brush cells in marmoset cerebellum and cochlear nuclei express calbindin. *Neuroreport* 11:1–4.
- Spatz WB. 2001. Unipolar brush cells in the human cochlear nuclei identified by their expression of a metabotropic glutamate receptor (mGluR2/3). *Neurosci Lett* 316:161–164.
- Spatz WB. 2003. Purkinje-like cells in the cochlear nucleus of the common tree shrew (*Tupaia glis*) identified by calbindin immunohistochemistry. *Brain Res* 983:230–232.
- Sternberger LA, Sternberger NH. 1983. Monoclonal antibodies distinguish phosphorylated and nonphosphorylated forms of neurofilaments in situ. *Proc Natl Acad Sci USA* 80:6126–6130.
- Valtschanoff JG, Weinberg RJ, Kharazia VN, Schmidt HH, Nakane M, Rustioni A. 1993. Neurons in rat cerebral cortex that synthesize nitric oxide: NADPH diaphorase histochemistry, NOS immunocytochemistry, and colocalization with GABA. *Neurosci Lett* 157:157–161.
- Valtschanoff JG, Weinberg RJ, Rustioni A, Schmidt HH. 1995. Colocalization of neuronal nitric oxide synthase with GABA in rat cuneate nucleus. *J Neurocytol* 24:237–245.
- Van der Gucht E, Hof PR, Van Brussel L, Burnat K, Arckens L. 2007. Neurofilament protein and neuronal activity markers define regional architectonic parcellation in the mouse visual cortex. *Cereb Cortex* 17:2805–2819.
- Van der Gucht E, Youakim M, Arckens L, Hof PR, Baizer JS. 2006. Variations in the structure of the prelunate gyrus in Old World monkeys. *Anat Rec* 288:753–775.
- Wagoner JL, Kulesza RJ, Jr. 2009. Topographical and cellular distribution of perineuronal nets in the human cochlear nucleus. *Hear Res* 254:42–53.
- Wang H, Brozoski TJ, Caspary DM. 2011. Inhibitory neurotransmission in animal models of tinnitus: maladaptive plasticity. *Hear Res* 279:111–117.
- Warchol ME, Speck JD. 2007. Expression of GATA3 and tenascin in the avian vestibular maculae: normative patterns and changes during sensory regeneration. *J Comp Neurol* 500:646–657.
- Witelson SF, McCulloch PB. 1991. Premortem and postmortem measurement to study structure with function: a human brain collection. *Schizophr Bull* 17:583–591.
- Wouterlood FG, Mugnaini E, Osen KK, Dahl AL. 1984. Stellate neurons in rat dorsal cochlear nucleus studies with combined Golgi impregnation and electron microscopy: synaptic connections and mutual coupling by gap junctions. *J Neurocytol* 13:639–664.
- Yang Z, You Y, Levison SW. 2008. Neonatal hypoxic/ischemic brain injury induces production of calretinin-expressing interneurons in the striatum. *J Comp Neurol* 511:19–33.
- Yeo EJ, Cho YS, Paik SK, Yoshida A, Park MJ, Ahn DK, Moon C, Kim YS, Bae YC. 2010. Ultrastructural analysis of the synaptic connectivity of TRPV1-expressing primary afferent terminals in the rat trigeminal caudal nucleus. *J Comp Neurol* 518:4134–4146.
- Zettel ML, Carr CE, O'Neill WE. 1991. Calbindin-like immunoreactivity in the central auditory system of the mustached bat, *Pteronotus parnelli*. *J Comp Neurol* 313:1–16.
- Zhang J, Guan Z. 2008. Modulatory effects of somatosensory electrical stimulation on neural activity of the dorsal cochlear nucleus of hamsters. *J Neurosci Res* 86:1178–1187.
- Zhang S, Oertel D. 1993a. Cartwheel and superficial stellate cells of the dorsal cochlear nucleus of mice: intracellular recordings in slices. *J Neurophysiol* 69:1384–1397.
- Zhang S, Oertel D. 1993b. Giant cells of the dorsal cochlear nucleus of mice: intracellular recordings in slices. *J Neurophysiol* 69:1398–1408.
- Zhang S, Oertel D. 1993c. Tuberculoventral cells of the dorsal cochlear nucleus of mice: intracellular recordings in slices. *J Neurophysiol* 69:1409–1421.
- Zook JM, Casseday JH. 1982. Cytoarchitecture of auditory system in lower brainstem of the mustache bat, *Pteronotus parnelli*. *J Comp Neurol* 207:1–13.